AD_____

Award Number: W81XWH-06-1-0116

TITLE: Role of Caveolin-1 in Prostate Cancer Angiogenesis

PRINCIPAL INVESTIGATOR: Timothy C. Thompson, Ph.D.

CONTRACTING ORGANIZATION: M. D. Anderson Cancer Center
Houston Texas 77030

REPORT DATE: December 2007

TYPE OF REPORT: Annual

PREPARED FOR: U.S. Army Medical Research and Materiel Command
Fort Detrick, Maryland 21702-5012

REPORT DOCUMENTATION PAGE

Form Approved
OMB No. 0704-0188

1. REPORT DATE *(DD-MM-YYYY)*	**2. REPORT TYPE**	**3. DATES COVERED** *(From - To)*
01-12-2007	Annual	15 NOV 2006 - 14 NOV 2007

4. TITLE AND SUBTITLE

Role of Caveolin-1 in Prostate Cancer Angiogenesis

5a. CONTRACT NUMBER

5b. GRANT NUMBER
W81XWH-06-1-0116

5c. PROGRAM ELEMENT NUMBER

6. AUTHOR(S)
Timothy C. Thompson, Ph.D.

E-Mail: timthomp@mdanderson.org

5d. PROJECT NUMBER

5e. TASK NUMBER

5f. WORK UNIT NUMBER

7. PERFORMING ORGANIZATION NAME(S) AND ADDRESS(ES)

M. D. Anderson Cancer Center
Houston Texas 77030

8. PERFORMING ORGANIZATION REPORT NUMBER

9. SPONSORING / MONITORING AGENCY NAME(S) AND ADDRESS(ES)
U.S. Army Medical Research and Materiel Command
Fort Detrick, Maryland 21702-5012

10. SPONSOR/MONITOR'S ACRONYM(S)

11. SPONSOR/MONITOR'S REPORT NUMBER(S)

12. DISTRIBUTION / AVAILABILITY STATEMENT
Approved for Public Release; Distribution Unlimited

13. SUPPLEMENTARY NOTES

14. ABSTRACT
My laboratory relocated to M. D. Anderson Cancer Center on October 1, 2008. The move and transition was handled in a very efficient manner and we did not compromise our progress toward the goals of this project in any way. With only slight modifications Tasks 1-3 are on schedule and we are progressing toward our stated goals. Notable achievements for the past year of funding include comprehensive documentation that prostate cancer cell derived, secreted caveolin-1 is taken up by cancer cells and tumor associated endothelial cells (Tahir et al., Cancer Res 68: 731-739, 2008). This autocrine/paracrine activity of secreted caveolin-1 promotes malignant progression and provides an accessible therapeutic target. In pursuit of a clinical therapy based on this mechanism we have also shown that systemic delivery of caveolin-1 antiserum suppresses primary tumor growth and increases survival in an immunocompetent mouse model of prostate cancer (see Fig 5-7). In our view these results represent a paradigm shift in prostate cancer translational research.

15. SUBJECT TERMS
Prostate cancer, angiogenesis, caveolin-1

16. SECURITY CLASSIFICATION OF:			**17. LIMITATION OF ABSTRACT**	**18. NUMBER OF PAGES**	**19a. NAME OF RESPONSIBLE PERSON**
a. REPORT	**b. ABSTRACT**	**c. THIS PAGE**			USAMRMC
U	U	U	UU	22	**19b. TELEPHONE NUMBER** *(include area code)*

Table of Contents

Page

Introduction……..4

Body……..5

Key Research Accomplishments……..8

Reportable Outcomes……8

Conclusion……9

References……9

Appendices……9

INTRODUCTION

Background: Caveolin-1 (cav-1) is an important structural/regulatory molecule involved in many aspects of molecular transport and cell signaling. Cav-1 activities are dependent on protein level and cell context, yet an understanding of the biological consequences of inappropriate cav-1 expression in malignant cells has been elusive. We have shown previously that cav-1 up-regulation is associated with metastatic, androgen-insensitive prostate cancer. In studies funded by this grant we identified an underlying mechanism for the selection of cav-1 overexpression in prostate cancer cells during progression. We found that cav-1 binds to and inhibits the activities of PP1/PP2A serine / threonine phosphatases, preventing inactivation of Akt through dephosphorylation and thus sustaining levels of phospho-Akt and its oncogenic activities. Recently we have shown that cav-1 overexpression leads to increased levels of c-myc protein, and our preliminary data and the results of published studies lead us to speculate that the mechanisms for cav-1 mediated c-myc stabilization also involve PP1/PP2A inhibition and phospho-Akt stabilization. We have also shown that cav-1 overexpression leads to up-regulation and secretion of VEGF, FGF2 and TGF-β1, indicating that cav-1 stimulated molecular pathways can regulate these growth factors (GF) /angiogenic cytokines (AC). Importantly, we have also discovered that cav-1 itself is specifically secreted by prostate cancer cells and is taken up by prostate cancer cells and endothelial cells (EC).

Hypothesis: These results suggest that cells expressing cav-1 can function as "feeder cells" for local and potentially distant prostate cancer cells and tumor-associated EC through secretion of cav-1 and cav-1 stimulated GF/AC. In support of this concept we have shown that experimentally induced metastasis is potentiated in host transgenic mice that overexpress cav-1 in and secrete cav-1 from prostatic epithelium. In contrast experimental metastasis is suppressed in host *cav-1*$^{-/-}$ mice compared to *cav-1*$^{+/+}$ mice. We propose that prostate cancer cells secrete cav-1 which induces specific changes in EC that potentiate angiogenesis and metastatic activities.

Specific Aims: Using in vitro and in vivo models that involve novel genetically mutant mice we propose to resolve the molecular and cellular pathways that support these oncogenic activities through specific aims to: (1) to analyze the effects of cav-1 conditioned media on cav-1$^{-/-}$ endothelial cell gene expression and biological activity; (2) map the molecular pathways involved in EC angiogenesis stimulated by cav-1 protein alone or together with specific GF/AC; and (3) to correlate the effects of prostate cancer cell derived cav-1 uptake by TAEC with tumor growth activities.

Study Design: We have generated and characterized mice that have a deletion of the *cav-1* gene. These will be a source for isolation of EC that will be treated with conditioned media derived from prostate cancer cells with controlled levels of cav-1 protein (Aim 1) or with purified cav-1 protein (Aim 2). We will determine the molecular events that are induced by cav-1 in EC by analyzing expression of signalling molecules such as phosphorylated Akt, c-myc and relevant GF/AC (VEGF, FGF-2, and TGF-β1) at the transcription level by quantitative RT-PCR and at the protein level by western blotting. Additionally we will evaluate events further downstream of signaling such as nitric oxide (NO) production. Biological activities of the EC in response to cav-1 that we will examine will include proliferation, chemoattraction, motility and vasculogenesis. The validation of these activities will be accomplished by using specific molecular inhibitors of the signaling molecules. The final aim of the grant will focus on in vivo studies using a novel mouse metastatic prostate cancer cell line that overexpresses cav-1 and has a high level of metastasis to lung and to bone. We will inject this cell line orthotopically (prostate) into *cav-1*$^{-/-}$ mice and then analyze TAEC responses locally and at distant sites of metastasis by immunohistochemistry. Treatment of the mice with cav-1 specific antibody will directly test the effects of blocking cav-1 uptake in vivo on the growth and progression of experimental prostate cancer in this model.

Relevance: These studies could lead to the use of cav-1 positive TAEC as a potential prognostic/ predictive biomarker for prostate cancer in man. They will further serve to test the therapeutic potential of cav-1 antibody approaches for the treatment of prostate cancer.

BODY

Task 1. ***To analyze the effects of cav-1 conditioned media (CM) on cav1$^{-/-}$ endothelial cell gene expression and biological activity***

1. Prepare EC from aorta of 40 *cav-1$^{-/-}$* and 20 *cav-1$^{+/+}$* mice and CM from cav-1 (500ml) or pcDNA (500ml) transfected LP-LNCaP cells.
   (Months 1-3)
2. Perform western blotting and QRT-PCR on EC lysates treated with cav-1 CM. (Months 3-18)
3. Develop biological assays for the EC activity (Motility/invasion, migration, tubule formation, NO and PGI2 determination) and analyze the effect of soluble cav-1 on these activities.
   (Months 18-36)

Mutagenesis experiments have identified the cav-1 scaffolding domain (CSD) residues 82-101 as the region of cav-1 responsible for mediating the interaction with a number of signaling proteins including eNOS, platelet activating factor (PDGF) receptors, epidermal growth factor (EGF), the kinases Src and Fyn, heterotrimeric G-protein and cholesterol binding. Therefore we constructed cav-1 plasmid with deleted CSD termed phΔcav-1-V5-His, and prepared CM from phΔcav-1-V5-His transfected LNCaP cells. The use of recombinant protein with deleted CSD (rΔcav-1) as well as CM will be important to investigate the role of CSD in the secretion, uptake and angiogenic activities of ECs.

Fig. 1: Rcav-1, but not Δrcav-1 stimulates angiogenic activities

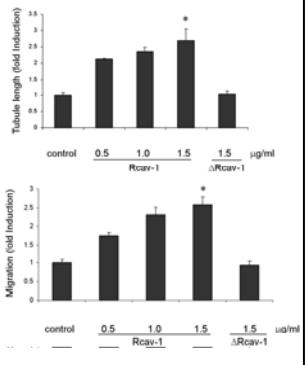

Fig. 2: Rcav-1, but not Δrcav-1 increase eNOS phosphorylation (S1177).

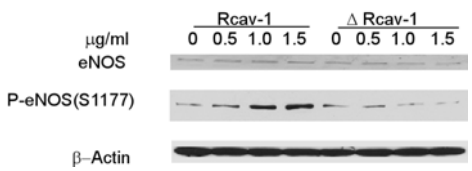

To determine the role of the CSD in exogenous rcav-1 membrane attachment and cellular uptake, we generated and purified the CSD deleted rcav-1 protein (Δrcav-1), treated EC and prostate cancer cells with different concentrations of FITC-Δrcav-1 over 1-6 h, and examined the cells for Δrcav-1 uptake using fluorescence microscopy. We did not detect internalized FITC-Δrcav-1 in cells incubated for as long as 6 h at concentrations of the mutant protein ranging to 5.0μg/ml. As expected, Δrcav-1 at concentrations up to 1.5 μg/ml failed to stimulate tubule formation and migration in *cav-1$^{-/-}$* EC (Fig 1), and eNOS phosphorylation at S1177 (Fig 2). These observations suggest that endocytosis of exogenous rcav-1 protein and its subsequent stimulation of angiogenic activities is mediated, in part, by CSD, which appears critical for cellular internalization of the protein.

The study of protein expression using western blotting and gene expression using QRT-PCR in EC lysates treated with cav-1 CM is underway. We recognize that we are making slow progress in this area, and that is primarily due to the difficulties in producing large quantities of primary *cav-1$^{-/-}$* and *cav-1$^{+/+}$* EC sufficient for these studies .

Task 2. ***Map the molecular pathways involved in EC angiogenesis stimulated by cav-1 protein alone or together with specific GF/AC.***

1. Preparation/purchase of reagents, including recombinant cav-1, VEGF, FGF-2, TGF-β1, siRNA for VEGFR2, PI3-K, Akt, ERK1/2 and eNOS, chemical inhibitors for VEGFR2, PI3-K, ERK1/2 and eNOS.
   (Months 1-3)
2. Optimize conditions for siRNA transfection and for chemical inhibitions.
   (Months 1-6)
3. Analysis of gene knock down, including QRT-PCR analysis for mRNA and western analysis for protein. Analysis range covers target genes and their downstream components.
   (Months 7-24)
4. Biological function end points.
   (Months 25-36)

Fig. 3: Rcav-1 inhibits the activity of PP2A but not PP1 in *cav-1*$^{-/-}$ EC.

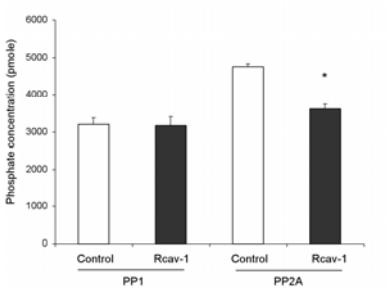

We are currently investigating different siRNA transfection protocols to find the highest transfection efficiency with primary mouse aortic endothelial cells. We tested trnasfection protocols from Santa Cruze Biotechnology, Ambion, and Lonza and we found that the Ambion amine transfection reagent produced the highest efficiency and we are currently developing procedures to further increase the efficiency to above 50% by changing the SiRNA concentrations, transfection reagents volume or the transfection time.

We have investigated the mechanism(s) that underlies rcav-1 stimulated eNOS activation by analyzing the effect of rcav-1 on the activities of two serine/threonine protein phosphatases PP1 and PP2A in *cav-1*$^{-/-}$ EC. These two phosphatases are known to regulate the phosphorylation of multiple protein targets including Akt and eNOS. We found that rcav-1 treatment significantly inhibited the activity of PP2A but had no effect on PP1 activity (P=0.0002 versus control, Fig 3) indicating that rcav-1 induces eNOS phosphorylation through Akt activation (previous progress report), and independently of Akt, through inhibition of PP2A which specifically dephosphorylates eNOS (S1177).

Additionally, we investigated the role played by cav-1 in compartmentalization of the PI-3-K-Akt-eNOS signaling pathway molecules in *cav-1*$^{-/-}$ EC, and found that Akt was not colocalized with eNOS in untreated cells, whereas significant colocalization of the two molecules was observed in the cells treated with rcav-1 (Fig 4).

The study of gene expression using QRT-PCR and proteins expression using western blotting in EC lysates treated with rcav-1 and/or GF is underway.

Fig. 4: Induction of eNOS/Akt association by rcav-1

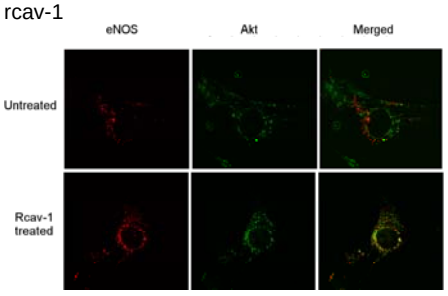

Task 3. To correlate the effects of prostate cancer cell derived cav-1 uptake by TAEC with tumor growth activities.

1. Inject 178-2 BMAK cells into dorsolateral prostate of twenty *cav-1*$^{-/-}$ mice and analyze tumor weight and metastasis at 21 day, fixed time point. Analyze tissues by immunohistochemistry
   (Months 1-12)
2. Inject 178-2 BMAK cells into dorsolateral prostate of thirty nine *cav-1*$^{-/-}$ mice then treat with HBSS, rabbit IgG, or rabbit anti-cav-1 serum (thirteen per group) and analyze tumor weight and metastasis at 21 day, fixed time point (12-18 months). Analyze tissues by immunohistochemistry
   (Months 12-36)
3. Inject 178-2 BMAK cells into dorsolateral prostate of thirty *cav-1*$^{-/-}$ mice then treat with HBSS, rabbit IgG, or rabbit anti-cav-1 serum (ten per group) and analyze tumor weight and metastasis at survival time point (12-18 months). Analyze tissues by immunohistochemistry
   (Months 12-36)

As we explained in our previous report due to minor histocompatibility problems and poor "take" of 178-2BMAK cells in *cav1*$^{-/-}$mice we replaced 178-2BMAK cells with RM-9 prostate cancer cells that were originally isolated from C57/BL6 mice. We have previously demonstrated that RM-9 cells secrete cav-1 into conditioned media in vitro and can be used in the orthotopic mouse prostate cancer model in vivo.

To test for anti-metastatic potential and the therapeutic effects of cav-1 antibodies in *cav-1*$^{-/-}$ mice we have modified our mouse model of metastatic prostate cancer by simultaneous administration of RM-9 prostate cancer cells through two different routes. A cohort of adult male *cav-1*$^{-/-}$ mice were injected with 5000 RM-9 cells into dorsolateral prostate to establish orthotopic prostate tumor and intravenously (tail vein) to establish experimental lung metastases. Two days after RM-9 cells injection mice were divided into 3 treatment groups and received IP injection (q/o/d) of anti cav-1 IgG, control IgG or HBSS. Mice were sacrificed at 21 days after initial tumor cells injection and prostate and lung tissues were collected for further analysis. Wet prostate tumor weight was significantly reduced in *cav-1*$^{-/-}$ mice that received anti-cav-1 IgG compared to the mice treated with control IgG or HBSS only (Fig.5). Treatment with anti-cav-1 IgG also had an anti-metastatic effect in cav-1$^{-/-}$ model and reduces number of metastatic lung metastasis compared to the control treatment groups (Fig. 6). Interestingly, in the same experimental setting the adult male *cav-1*$^{-/-}$ mice received anti-cav-1 IgG survived significantly longer then cav-1$^{-/-}$ littermate treated with control IgG or HBSS only (Fig.7). Thus, anti-cav-1 IgG can significantly reduce local tumor growth as well as experimental metastasis most likely by reducing systemic cav-1 levels secreted by RM-9 prostate tumor cell. This experiment also suggests that anti-cav-1 IgG can be potentially novel systemic therapeutic modality for the treatment of metatstatic prostate cancer. We will analyze collected tissues for any changes in GF/AC related to cav-1 or anti-cav-1 IgG treatment.

Fig. 5: Anti-cav-1 antibody treatment significantly reduces the wet weight of orthotopic RM-9 tumors grown in cav-1$^{-/-}$ mice compare to control IgG or HBSS groups (* P < 0.05)

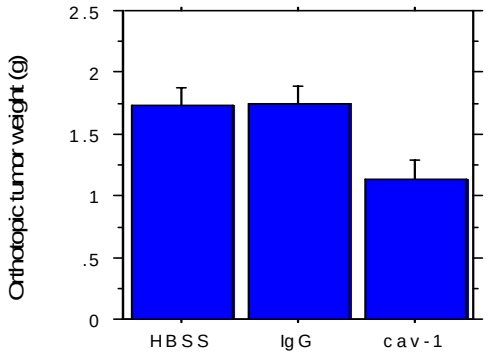

Fig. 6: Anti-cav-1 antibody treatment significantly reduces the number of RM-9 experimental lung metastases tumors in cav-1$^{-/-}$ mice compare to control IgG or HBSS groups (* P < 0.05)

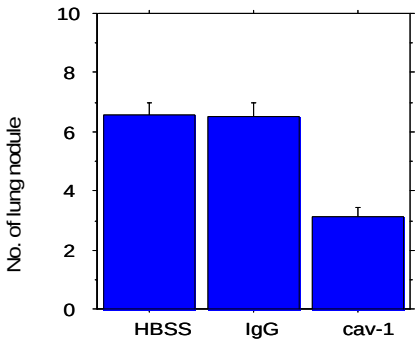

Fig. 7 : The cav-1$^{-/-}$ mice with orthotopic RM-9 tumor and lung metastases treated with anti-cav-1 antibody survive significantly longer compare to mice treated with control IgG or HBSS (Kaplan-Meier survival plot)

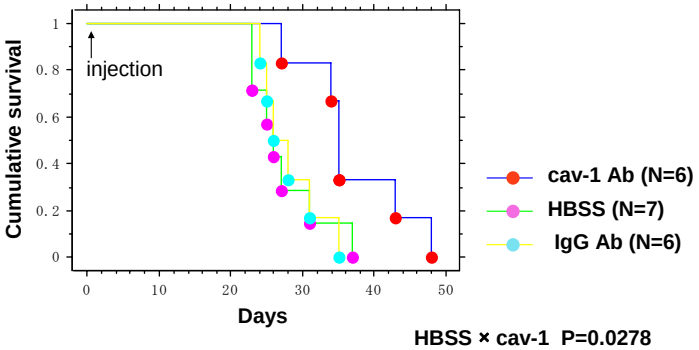

Significance:
Thus far our new mechanistic data are consistent with the concept that angiogenic activities of prostate cancer cell derived, secreted cav-1 promotes tumor progression. In our view, this novel concept will lead to novel approaches for prostate cancer diagnosis and therapy.

Plans:
In general our experiments are on track and yielding important and interesting results. Since last year we have published two important papers demonstrating cav-1 mediated angiogenic activity in prostate cancer. In the current year we anticipate to collect all the remaining experimental data to conclude the studies planned and supported by this grant.

Publications:
1. Tahir ST, Frolov A, Hayes TG, Mims, MP, Miles BJ, Lerner SP, Wheeler TM, Ayala G, Wheeler TM, Thompson TC and Kadmon D**.** Preoperative serum caveolin-1 as a prognostic marker for recurrence in a radical prostatectomy cohort. Clin Can Res, 12(16):4872-4875, 2006.
2. Yang G, Addai J, Wheeler TM, Frolov A, Miles BJ, Kadmon D and Thompson TC. Correlative evidence that prostate cancer cell-derived caveolin-1 mediates angiogenesis. Hum Pathol. 2007 Nov;38(11):1688-95.
3. Tahir SA, Yang G, Goltsov AA, Watanabe M, Tabata K, Addai J, Abdel Fattah E Kadmon D and Thompson TC. Tumor cell-secreted caveolin-1 has proangiogenic activities in prostate cancer. Cancer Res 68(3): 731-739, 2008.

KEY RESEARCH ACCOMPLISHMENTS
1. Secreted cav-1 stimulates angiogenic activities in *cav-1*$^{-/-}$ mouse EC.
2. Akt (S473, T308) and eNOS (S1177) are significantly phosphorylated in rcav-1 treated *cav-1*$^{-/-}$ mouse EC.
3. Rcav-1, but not Δrcav-1 stimulates the phosphorylation of eNOS on S1177 and angiogenic activities in *cav-1*$^{-/-}$ mouse EC.
4. Administration of anti-cav-1 IgG significantly reduce local tumor growth as well as experimental metastasis most likely by reducing systemic cav-1 levels secreted by RM-9 prostate tumor cell.

REPORTABLE OUTCOMES
Presentations:
1. Tahir SA, Yang G, Goltsov A, Watanabe M, Tabata K, and Thompson TC. Caveolin-1 uptake by endothelial cells promotes angiogenic activities and is associated with prostate cancer progression. American Association for Cancer Research, 97th Annual Meeting, Washington DC, April 1-5, 2006.
2. Tahir SA, Yang G, Goltsov A, Watanabe M, Tabata K and Thompson TC. Caveolin-1 uptake by endothelial cells promotes angiogenic activities and is associated with prostate cancer progression. 4th Annual Cancer Center Symposium, Houston, TX, November 3, 2006.
3. Miles BJ, Yang G, Addai J, Wheeler TM, Frolov A, Kadmon D and Thompson TC. Correlative evidence that prostate cancer cell-derived caveolin-1 mediates angiogenesis. American Society of Clinical Oncology annual meeting, June 1 – 5, 2007, Chicago, IL.
4. Thompson TC. U.S. Department of Defense, Prostate Cancer Research Program (PCRP) Innovative Minds in Prostate Cancer Today (IMPaCT), Thursday, September 5-8, 2007, Atlanta, Georgia. "Caveolin-1 Uptake and Pro-angiogenic Activities in Prostate Cancer".

Manuscripts:
1. Yang G, Addai J, Wheeler TM, Frolov A, Miles BJ, Kadmon D and Thompson TC. Correlative evidence that prostate cancer cell-derived caveolin-1 mediates angiogenesis. Hum Pathol. 2007 Nov;38(11):1688-95.
2. Tahir SA, Frolov A, Hayes TG, Mims, MP, Miles BJ, Lerner SP, Wheeler TM, Ayala G, Wheeler TM, Thompson TC and Kadmon D**.** Preoperative serum caveolin-1 as a prognostic marker for recurrence in a radical prostatectomy cohort. Clin Can Res, 12(16):4872-4875, 2006.

3. Tahir SA, Yang G, Goltsov AA, Watanabe M, Tabata K, Addai J, Abdel Fattah E Kadmon D and Thompson TC. Tumor cell-secreted caveolin-1 has proangiogenic activities in prostate cancer. Cancer Res 68(3): 731-739, 2008.

CONCLUSION

Overall, we have made exceptional progress in the first year funding period of this project. Tasks 1-3 are on schedule and although, as is often the case, we have made some unanticipated and necessary adjustments (replacement of 178-2BMAK cells with RM-9 cells for Task 3) we are moving toward our stated goals. Importantly, our data thus far, are yielding important mechanistic insight into the angiogenic activities of prostate cancer cell derived, secreted cav-1. In our view, after we further define these mechanisms we will be able to take the next important step, exploiting this new knowledge for prostate cancer diagnosis and therapy.

REFERENCES

None cited in text

APPENDICES

Tahir ST, Frolov A, Hayes TG, Mims, MP, Miles BJ, Lerner SP, Wheeler TM, Ayala G, Wheeler TM, Thompson TC and Kadmon D**.** Preoperative serum caveolin-1 as a prognostic marker for recurrence in a radical prostatectomy cohort. Clin Can Res, 12(16):4872-4875, 2006.

Tahir SA, Yang G, Goltsov AA, Watanabe M, Tabata K, Addai J, Abdel Fattah E Kadmon D and Thompson TC. Tumor cell-secreted caveolin-1 has proangiogenic activities in prostate cancer. Cancer Res 68(3): 731-739, 2008.

Preoperative Serum Caveolin-1 as a Prognostic Marker for Recurrence in a Radical Prostatectomy Cohort

Salahaldin A. Tahir,[1] Anna Frolov,[1] Teresa G. Hayes,[4] Martha P. Mims,[4] Brian J. Miles,[1] Seth P. Lerner,[1] Thomas M. Wheeler,[2] Gustavo Ayala,[2] Timothy C. Thompson,[1,3,5] and Dov Kadmon[1]

Abstract

Purpose: Up-regulation of caveolin-1 (cav-1) is associated with virulent prostate cancer, and serum cav-1 levels are elevated in prostate cancer patients but not in benign prostatic hyperplasia. In this study, we evaluated the potential of high preoperative serum cav-1 levels to predict biochemical progression of prostate cancer. The value of the combined preoperative markers, prostate-specific antigen (PSA), biopsy Gleason score, and serum cav-1 for predicting biochemical recurrence was also investigated.

Experimental Design: Serum samples taken from 419 prostate cancer patients before radical prostatectomy were selected from our Specialized Programs of Research Excellence prostate cancer serum and tissue bank. Serum samples were obtained 0 to 180 days before surgery and all patients had complete data on age, sex, race, stage at enrollment, and follow-up for biochemical recurrence. Serum cav-1 levels were measured according to our previously reported ELISA protocol.

Results: Cav-1 levels were measured in the sera of 419 prostate cancer patients; the mean serum level was 4.52 ng/mL (median 1.01 ng/mL). Patients with high serum cav-1 levels had a 2.7-fold ($P = 0.0493$) greater risk of developing biochemical recurrence compared with those with low serum cav-1 levels. Importantly, patients with serum PSA $\geq$ 10 ng/mL and elevated levels of serum cav-1 had 2.44 times higher risk ($P = 0.0256$) of developing biochemical recurrence compared with patients with low levels of cav-1. In addition, high serum cav-1 levels combined with increasing biopsy Gleason score predicted much shorter recurrence-free survival in the group of patients with PSA $\geq$ 10 ng/mL ($P = 0.0353$). Cav-1 was also able to distinguish between high- and low- risk patients with biopsy Gleason score of seven, after adjusting, for patients PSA levels ($P = 0.0429$).

Conclusions: Overall, elevated preoperative levels of serum cav-1 predict decreased time to cancer recurrence. In the subset of patients with serum PSA of $\geq$10 ng/mL, the combination of serum cav-1 and biopsy Gleason score has the capacity to predict time to biochemical recurrence.

In 2005, ~90% of newly diagnosed prostate cancer patients had clinically localized disease (1). Consequently, the majority of patients are treated with curative intent by either radical prostatectomy or radiation therapy. It is well established, however, that 10% to 50% of patients who undergo radical prostatectomy will show biochemical evidence of disease recurrence [prostate-specific antigen (PSA) recurrence] within 5 years of surgery (2, 3). Various clinical variables have been used, singly and in combination (nomograms, tables, etc.), to predict, preoperatively, which patients are likely to fail definitive therapy (4). However, the predictive value of these variables has been thwarted by the vexing biological diversity of clinical prostate cancer. New markers are needed, preferably serum markers that have been mechanistically implicated in the progression of virulent disease. We believe that serum caveolin-1 (cav-1) may be such a marker.

Cav-1 is an important structural/regulatory molecule involved in many aspects of molecular transport and cell signaling (5, 6). Tissue cav-1 is overexpressed in metastatic and in hormone-resistant prostate cancer (7). Overexpression correlates with a shortened interval to disease recurrence following therapy for localized disease and tends to be associated with a high Gleason score pathologically (8–10). Interestingly, cav-1 is secreted by prostate cancer cells (11) and we have developed a sensitive ELISA immunoassay for the detection of cav-1 in the serum (12). In a preliminary study, we documented that prostate cancer patients have a higher serum cav-1 level when compared with age-matched controls with benign prostatic hyperplasia (12).

We report here the utility of a single preoperative measurement of serum cav-1 for predicting disease recurrence in a cohort of 419 prostate cancer patients undergoing radical prostatectomy at our institution.

Authors' Affiliations: [1]Scott Department of Urology and Departments of [2]Pathology, [3]Radiology, [4]Medicine, and [5]Molecular and Cellular Biology, Baylor College of Medicine, Houston, Texas

Received 2/21/06; revised 3/31/06; accepted 4/20/06.

Grant support: National Cancer Institute Specialized Programs of Research Excellence grants P50-58204 and RO1-68814.

The costs of publication of this article were defrayed in part by the payment of page charges. This article must therefore be hereby marked *advertisement* in accordance with 18 U.S.C. Section 1734 solely to indicate this fact.

Requests for reprints: Dov Kadmon, Scott Department of Urology, Baylor College of Medicine, 6560 Fannin, Suite 2100, Houston, TX 77030. E-mail: dkadmon@bcm.tmc.edu.

doi:10.1158/1078-0432.CCR-06-0417

Materials and Methods

Study population. The sera of 419 prostate cancer patients were obtained from the Specialized Programs of Research Excellence prostate cancer blood and tissue bank at Baylor College of Medicine. Entry into the study required availability of preoperative serum samples obtained within 6 months of surgery and complete data on age, race, stage at enrollment and follow-up, as well as availability of postoperative serum samples, as this is a part of a larger ongoing investigation. In addition, patients could have had no preoperative therapy. After completion of cav-1 measurements in the serum, it was discovered that seven patients were missing reliable data on their preoperative PSA and/or biopsy Gleason score and/or follow-up information. These patients were included in all analyses that did not require missing data. The preoperative serum collected from 355 patients was at a time period between prostate biopsy and surgery. No information was available in our database on the exact preoperative serum collection timing with respect to biopsy for 64 patients. The mean age of this patient group was 62.6 years (range 42.6-78.9 years); 91.4% were White males, with Hispanics, African-Americans, and Asians comprising 6.0%, 2.4%, and 0.2%, respectively. Mean follow-up time among this group of patients was 52 months, with a median follow-up time of 48 months. Biochemical recurrence is defined throughout this study as serum PSA level of $\geq$0.2 ng/mL on two consecutive measurements, using the first-generation postresection PSA assay (Hybritech, Beckman Coulter, Inc., Fullerton, CA). Patient data were gathered from the Informatics Core using the Specialized Programs of Research Excellence in Prostate Cancer Information System.

Determination of serum cav-1. Cav-1 was determined in the serum samples by the sandwich ELISA protocol developed in our laboratory (12). Briefly, Costar microplate wells were coated with 0.5 μg cav-1 polyclonal antibody (Transduction Laboratories, San Diego, CA) and blocked with TBS buffer containing 1.5% bovine serum albumin and 0.05% v/v Tween 20. Serum samples, calibrators, and controls (50 μL) were added to the well, and 50 μL TBS containing 0.5% v/v Tween 20 was added to each well. The plate was incubated at room temperature for 2 hours with shaking and after extensive washing, 100 μL horseradish peroxidase–conjugated cav-1 antibody (Santa Cruz Biotechnology, Santa Cruz, CA) diluted 1:200 in blocking buffer was added to each well. The microplate was incubated for 90 minutes at room temperature with shaking, the wells were then washed extensively, and 100 μL 3,3′,5,5′-tetramethylbenzidine substrate solution (Sigma-Aldrich, St. Louis, MO) was added and the blue color was allowed to develop for 20 minutes in the dark. The reaction was stopped by adding 50 μL of 2 N H_2SO_4, and the absorbance was read at 450 nm using a microplate reader (Sunrise Microplate Reader, Tecan US, Inc., Charlotte, NC).

Statistical analysis. Correlations of preoperative serum cav-1 levels with clinical and pathologic variables were evaluated using the Spearman correlation. The predictive value of cav-1 univariately and multivariately with other preoperative clinical and pathologic variables, such as preoperative PSA and biopsy Gleason score, as well as of the interactive terms, were analyzed using the Cox proportional hazards regression model. The minimum *P* value method was used to group patients into "low-level" and "high-level" cav-1 categories (13). The hazard ratio (HR) and 95% confidence intervals (95% CI) were computed for each marker. Kaplan-Meier survival curves were plotted for each risk category. $P < 0.05$ was considered statistically significant. All analyses were done using the SPSS 12.0 software package (SPSS, Inc., Chicago, IL)

Table 1. Preoperative serum cav-1 level correlation with clinical and pathologic variables

	n	Mean (range), %	r^2	*P*
Preoperative cav-1	419	4.5 (0.0-156.7)	—	—
Preoperative PSA (ng/mL)	415	8.6 (0.4-53.2)	0.01	0.9013
Age	419	62.6 (42.6-78.9)	0.02	0.6268
Biopsy Gleason score	412	6.1 (3-9)	−0.06	0.2051
Seminal vesicle invasion	419	7.6%	−0.01	0.8543
Lymph node involvement	419	3.8%	0.08	0.1024
Extraprostatic extension	419	32.7%	0.07	0.1378
Margin positive	419	11.9%	0.06	0.2425
Gleason score	419	6.5 (3-9)	−0.01	0.8342

Table 2. Preoperative serum cav-1 is a univariate and multivariate predictor of decreased biochemical recurrence-free survival

	HR (95% CI)	*P*
Univariate model		
Preoperative cav-1	2.78 (1.003-7.70)	0.0493
Multivariate model		
Preoperative cav-1	2.57 (0.92-7.12)	<0.0704
Ln(PSA)	2.31 (1.60-3.33)	<0.0001
Biopsy Gleason score	1.74 (1.32-2.30)	0.0001

Results

Serum cav-1 levels were measured in 419 prostate cancer patients. The mean cav-1 value was 4.52 ng/mL and the median level was 1.01 ng/mL (range 0.0-156.7 ng/mL). Serum cav-1 levels seemed to have a bimodal distribution, with positive values distributed log normally. The serum cav-1 levels were analyzed for correlation with other pathologic and clinical variables using the Spearman correlation. No statistically significant correlations with clinicopathologic variables were found (Table 1).

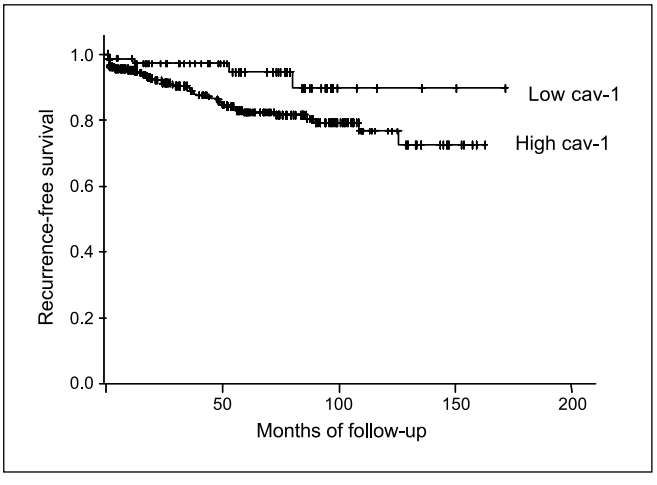

Fig. 1. High expression of cav-1 predicts decreased biochemical recurrence-free survival. This Kaplan-Meier plot illustrates the differences in recurrence-free survival between the low and high groups when separated by cav-1 cut point of 0.13 ng/mL. Patients with high level of cav-1 experienced significantly higher risk of recurrence than those with low levels ($P = 0.0493$).

There were 414 patients with complete follow-up information were included in the analysis of recurrence-free survival (mean follow-up 52.3 months, maximum 171.3 months); 54 patients had PSA recurrence during follow-up. Although it was clear that patients with no or very low levels of cav-1 had a better prognosis, the optimal cutoff was selected using the minimum *P* value method (13). This defined the low cav-1 group as patients with levels of <0.13 ng/mL and the high cav-1 group as those with >0.13 ng/mL. In univariate analysis, the risk of experiencing biochemical recurrence, estimated by HR, was 2.8 times higher ($P = 0.0493$) for the high cav-1 group compared with the low cav-1 group (Table 2). Kaplan-Meier plots illustrate the shorter time to biochemical recurrence following radical prostatectomy in the high cav-1 group compared with low cav-1 group. The 5- and 10-year recurrence-free survival rates were 94.4% and 90.5% for the low cav-1 group compared with 82.0% and 71.8% for the high cav-1 group. This corresponds to a consistent 12% to 21% increased progression-free survival for the low cav-1 group (Fig. 1). When the preoperative serum PSA level and the biopsy Gleason score were incorporated into the multivariate Cox proportional hazard model, the recurrence risk was 2.6 times higher for the high cav-1 group, but this effect was just below the level of significance ($P = 0.0704$; Table 2).

The effect of the serum cav-1 level on biochemical recurrence was further analyzed in patients with more advanced cancers, characterized by PSA of ≥10 ng/mL. The distribution shape remained the same and patients with low cav-1 levels continued to have a better prognosis. A new optimal cutoff of 2.86 ng/mL was identified for this subgroup of patients. Univariately, the estimated risk of recurrence was 2.44 times higher ($P = 0.0256$) in the high cav-1 group (serum cav-1 >2.86 ng/mL) than in its low cav-1 counterpart (serum cav-1 ≤ 2.86 ng/mL; Table 3). Kaplan-Meier plots illustrate that patients in the high cav-1 group had a much shorter time to recurrence than those in the low cav-1 group (Fig. 2). This figure also indicates a 10-year recurrence-free survival rate of 70.3% in the low cav-1 group compared with 47.4% in the high cav-1 group corresponding to a >20% decrease in progression-free survival in the low cav-1 group.

Incorporating the biopsy Gleason score into the Cox proportional hazard model (Table 3), we found that the interaction term between Gleason score and the cav-1 was the most predictive ($P = 0.0353$). This indicates that the biopsy Gleason score was an additional risk factor only in the high cav-1 group. The Kaplan-Meier plot (Fig. 3) illustrates this result by showing the highest recurrence risk in patients with high cav-1 and high biopsy Gleason score (7–9); and lower

Table 3. Preoperative serum cav-1 is a univariate and multivariate predictor of decreased biochemical recurrence-free survival among patients with preoperative PSA of ≥10

	HR (95% CI)	*P*
Univariate model		
Preoperative cav-1	2.44 (1.12-5.34)	0.0256
Multivariate model		
Preoperative Cav-1 × biopsy Gleason score	1.13 (1.01-1.27)	0.0353

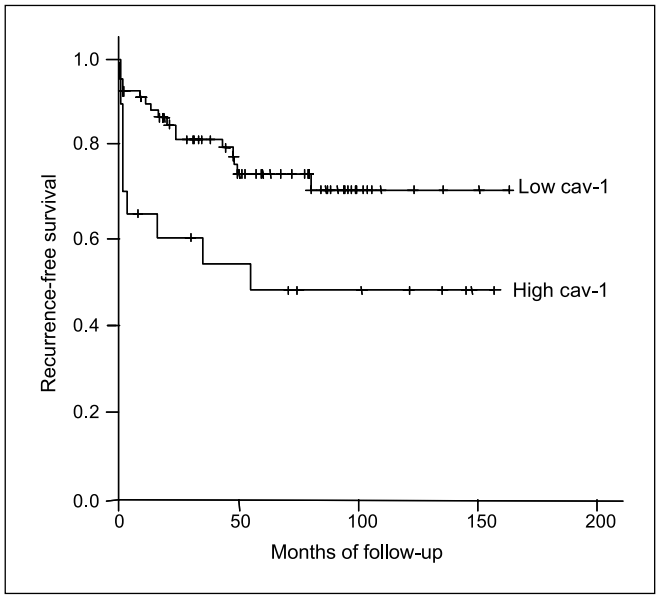

Fig. 2. For patients with PSA of ≥10, high expression of cav-1 is a strong predictor of decreased biochemical recurrence-free survival. For this high-risk patient subgroup, optimal cutoff was determined to be at 2.86 ng/mL. The Kaplan-Meier plot here shows the difference observed in the data.

recurrence risk in the high cav-1 and low biopsy Gleason score (<7) group, and those patients with low cav-1 regardless of the biopsy Gleason score. Recurrence-free survival curve for patients with low PSA (<10) was plotted for reference as well.

For biopsy Gleason 7 patients, the trend was the same: Higher cav-1 was observed in higher-risk patients. The difference in risk of recurrence, estimated by HR, between low and high cav-1 patients with cutoff defined at upper quartile of cav-1 (and confirmed by minimum *P* value method), was not statistically significant ($P = 0.0953$). However, after including preoperative PSA in the model, the

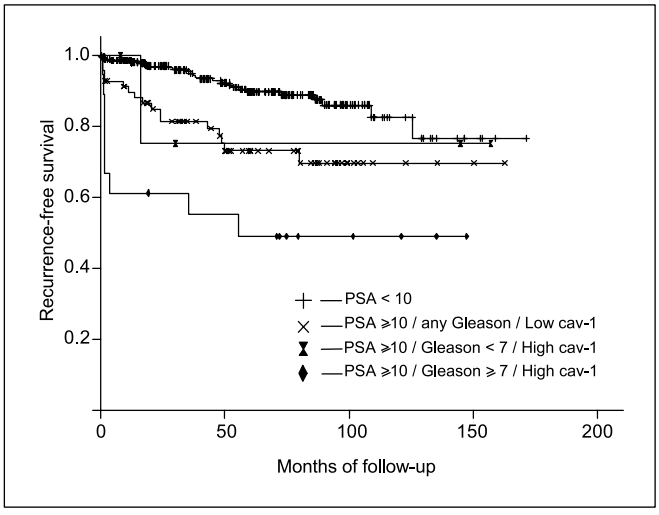

Fig. 3. Cav-1 works with biopsy Gleason score and preoperative PSA to predict biochemical recurrence-free survival. The interaction term between biopsy Gleason score and the cav-1, incorporated into the Cox proportional hazard, was the most predictive of recurrence-free survival among patients with PSA of ≥10 ($P = 0.0353$). This Kaplan-Meier plot illustrates how patients with both high cav-1 (>2.86 ng/mL) and biopsy Gleason score of ≥7 have the poorest prognosis. Curve for patients with PSA < 10 was plotted for reference.

difference became statistically significant (HR, 2.29; P = 0.0429). A patient with cav-1 in the upper quartile had over twice the risk of recurrence of one with cav-1 in the lower three quartiles if their preoperative PSA levels were the same.

Discussion

This study is part of our ongoing efforts to elucidate the biology and to define the clinical usefulness of serum cav-1 in prostate cancer. Although the factors modulating the serum levels of this biomarker remain largely unknown, the current study points out that a single preoperative serum cav-1 determination has prognostic value in a radical prostatectomy cohort. We observed the increase of the risk of biochemical recurrence with high levels of serum cav-1, and so we used the minimum P value method to segregate the patients into low-level and high-level groups. Remarkably, the risk of experiencing a PSA recurrence, estimated by HR, was 2.78 (95% CI, 1.003-7.70) times higher for the high-level cav-1 group (P = 0.0493), (see Fig. 1; Table 2). Incorporating the preoperative serum PSA level and the biopsy Gleason score into the model dropped the effect of cav-1 to just below the level of significance (HR, 2.57; P = 0.0704).

Interestingly, we found that the serum cav-1 levels are particularly important in predicting recurrence-free survival in patients with more advanced disease as defined by the preoperative serum PSA. When only patients with preoperative serum PSA levels of 10 ng/mL or higher were analyzed, cav-1 remained a significant predictor of recurrence-free survival (HR, 2.44; P = 0.0256). Additionally, the cav-1/biopsy Gleason score interaction term was a significant predictor (P = 0.0353). This implies that patients with both a high biopsy Gleason score and a high serum cav-1 level have a higher risk of biochemical recurrence than the remaining patients. Also, a subgroup of biopsy Gleason 7 prostate cancer patients, defined by the upper 25% of serum cav-1 levels, seems to harbor a biologically more aggressive prostate cancer after correction for individual PSA levels. All of these findings are consistent with our previous reports based on tissue up-regulation of cav-1 expression (8).

Notably, the distribution of the serum cav-1 values in the study population was not a normal distribution. About 10% of patients had undetectable serum levels by our sensitive ELISA essay. We can only speculate at this point as to the possible reason for this phenomenon. It is possible that the presence of any cav-1 in the serum is dictated by the genetic background of the individual and that, physiologically, there may be "secretors" and "nonsecretors." Within the secretor population, the specific makeup of the cancer may be contributing to the absolute serum level.

Surprisingly, we could not correlate the serum cav-1 levels with any of a large number of clinical and/or pathologic variables using the Spearman correlation (Table 1). We suggest that the reason is that cav-1 is an independent biomarker causally implicated in disease progression and not simply an epiphenomenon.

Many questions remain. For instance, we do not know the incidence of false-positive and/or false-negative elevated serum cav-1 values vis-à-vis the tumor tissue cav-1 expression. Only a correlative study of tissue and serum levels of cav-1 can answer this question. Likewise, the kinetics of the serum cav-1 has not been worked out, nor do we know what the stability of serum cav-1 is over extended periods of time. Clearly, we are at the beginning of the road leading to the establishment of serum cav-1 as a prognostic marker for prostate cancer. The data presented here suggest that this road is worth pursuing.

References

1. Cooperberg MR, Moul JW, Carroll PR. The changing face of prostate cancer. J Clin Oncol 2005;23:8146–51.
2. Shipley WU, Thames HD, Sandler HM, et al. Radiation therapy for clinically localized prostate cancer: a multi-institutional pooled analysis. JAMA 1999;281:1598–604.
3. Bracarda S, de Cobelli O, Greco C, et al. Cancer of the prostate. Crit Rev Oncol Hematol 2005;56:379–96.
4. Chin JL, Reiter RE. Molecular markers and prostate cancer prognosis. Clin Prostate Cancer 2004;3:157–64.
5. Shaul PW, Anderson RG. Role of plasmalemmal caveolae in signal transduction. Am J Physiol 1998;275:L843–51.
6. Ikonen E, Parton RG. Caveolins and cellular cholesterol balance. Traffic 2000;1:212–7.
7. Nasu Y, Timme TL, Yang G, et al. Suppression of caveolin expression induces androgen sensitivity in metastatic androgen-insensitive mouse prostate cancer cells. Nat Med 1998;4:1062–4.
8. Yang G, Truong LD, Wheeler TM, Thompson TC. Caveolin-1 expression in clinically confined human prostate cancer: a novel prognostic marker. Cancer Res 1999;59:5719–23.
9. Satoh T, Yang G, Egawa S, et al. Caveolin-1 expression is a predictor of recurrence-free survival in pT_2N_0 prostate carcinoma diagnosed in Japanese patients. Cancer 2003;97:1225–33.
10. Yang G, Addai J, Ittmann M, Wheeler TM, Thompson TC. Elevated caveolin-1 levels in African-American versus White-American prostate cancer. Clin Cancer Res 2000;6:3430–3.
11. Tahir SA, Yang G, Ebara S, et al. Secreted caveolin-1 stimulates cell survival/clonal growth and contributes to metastasis in androgen-insensitive prostate cancer. Cancer Res 2001;61:3882–5.
12. Tahir SA, Ren C, Timme TL, et al. Development of an immunoassay for serum caveolin-1: a novel biomarker for prostate cancer. Clin Cancer Res 2003;9:3653–9.
13. Mazumdar M, Glassman JR. Categorizing a prognostic variable: review of methods, code for easy implementation and applications to decision-making about cancer treatments. Stat Med 2000;19:113–32.

Tumor Cell–Secreted Caveolin-1 Has Proangiogenic Activities in Prostate Cancer

Salahaldin A. Tahir,[1] Guang Yang,[1] Alexei A. Goltsov,[1] Masami Watanabe,[1] Ken-ichi Tabata,[1] Josephine Addai,[1] El Moataz Abdel Fattah,[1] Dov Kadmon,[1] and Timothy C. Thompson[1,2,3]

[1]Scott Department of Urology, Departments of [2]Molecular and Cellular Biology and [3]Radiology, Baylor College of Medicine, Houston, Texas

Abstract

Caveolin, a major structural component of specialized plasma membrane invaginations (caveolae) that participate in diverse cellular activities, has been implicated in the pathogenesis of several human diseases, including cancer. We showed in earlier studies that caveolin-1 (cav-1) is consistently and strongly overexpressed in metastatic prostate cancer and is secreted in a biologically active form by virulent prostate cancer cells. Using both *in vitro* and *in vivo* model systems, we now present evidence supporting a proangiogenic role for cav-1 in prostate cancer development and progression. Recombinant cav-1 (rcav-1) was taken up by cav-1$^{-/-}$ endothelial cells through either a lipid raft/caveolae- or clathrin-dependent mechanism, leading to specific angiogenic activities (tubule formation, cell migration, and nitric oxide production) that were mediated by rcav-1 stimulation of the PI3K-Akt-eNOS signaling module. Pathologic angiogenesis induced by cav-1 in prostate cancer–bearing mice correlated with an increased frequency, number, and size of lung metastases. We propose that in addition to its antiapoptotic role, cav-1 secreted by prostate cancer cells functions critically as a proangiogenic factor in metastatic progression of this tumor. These new insights into cav-1 function in prostate cancer may provide a base for the design of clinically applicable therapeutic strategies. [Cancer Res 2008;68(3):731–9]

Introduction

As essential components of caveolae, caveolin proteins help to generate and maintain these highly ordered structures at the cell surface. They also mediated endocytosis and transcytosis of molecules attached to the cell surface and organize signaling proteins involved in cell proliferation, adhesion, and migration, among numerous other biological processes (1). This functional versatility has focused increasing attention on the possible role of caveolins in cancer development and progression. Findings to date clearly indicate that caveolin-1 (cav-1), the first of several caveolin family members that differ in structure and tissue distribution, can influence both tumorigenesis and metastatic spread in certain types of cancer (2–6), although the mechanisms of these effects are largely unknown. We showed in earlier studies that cav-1 is consistently and strongly overexpressed in metastatic prostate cancer and is secreted in a biologically active form by virulent prostate cancer cells (2, 3, 7). Interestingly, we detected significantly increased serum cav-1 levels in prostate cancer patients compared with control men or men with benign prostatic hyperplasia, and showed that preoperative serum cav-1 is a potential prognostic marker for recurrence in radical prostatectomy cohort (8, 9). The ability of some prostate cancer cells to secrete biologically active cav-1 (7, 8), and the demonstration that loss of cav-1 function in the TRAMP transgenic mouse prostate cancer model results in highly significant reductions of prostate cancer growth and metastasis (10), led us to suspect that tumor cell–secreted cav-1 may function as a paracrine factor during prostate cancer development, possibly as a regulator of pathologic angiogenesis. The studies described here substantiate this role and suggest a paradigm that may be applicable to other tumors that secrete cav-1.

Materials and Methods

Endothelial cell isolation. Endothelial cells from *cav-1*$^{-/-}$ mice (11) were isolated from mouse aorta according to the primary explant procedure and used throughout the study. Briefly, the aorta was removed from the anaesthetized mice, placed in PBS, and carefully cleaned of periadventitial fat and connective tissue. The vessel was then cut into 1-mm pieces, opened longitudinally, and placed with the intima side down on Matrigel-coated (BD Biosciences) 12-well plates in endothelial cell growth medium (EGM; Cambrex) to generate endothelial outgrowth. The aortic pieces were removed after 4 to 7 days, and the cells were allowed to grow to confluence. After recovery with dispase, the cells were plated on a 12-well plate and then subcultured twice. The confluent monolayers showed the typical cobblestone pattern of endothelial cells stained positively for uptake of Dil-Ac-LDL (Biomedical Technologies).

Western blotting. Protein aliquots from cell lysates were separated by 10% or 12% SDS-PAGE and transferred to nitrocellulose membranes. The membranes were probed with antibodies to cav-1 (Santa Cruz Biotechnology), eNOS, Erk1/2, Akt (BD Biosciences), P-Akt, P-eNOS, or P-Erk1/2 (Cell Signaling Technology).

Recombinant cav-1 and Δrecombinant cav-1 purification. phCav-1V5 and phΔcav-1V5His plasmids were constructed as described previously (8), whereas recombinant cav-1 (rcav-1) and Δrcav-1 were purified by our modified procedure. Briefly, transfected 293PE cells were washed with PBS and lysed with 10 mL of ice-cold buffer A [50 mmol/L phosphate buffer, 300 mmol/L NaCl, 10 mmol/L imidazole, and 5 mmol/L mercaptoethanol (pH.8)] containing 0.5% Triton X-100 and 0.7% octylβ-D-glucopyranoside (OGP). The lysate was centrifuged for 15 min at 4°C, 12,000 × *g*, and the supernatant was mixed and incubated with 1 mL of Ni-NTA agarose slurry for 3 h. The resultant mixture was loaded on to a 10 mL polyprep column (Bio-Rad), and the resin was washed with 10 volumes of buffer A containing 500 mmol/L NaCl, 50 mmol/L imidazole, and 0.2% OGP. The bound cav-1-V5-His was eluted with 3 mL of elution buffer (buffer A containing 300 mmol/L imidazole, 300 mmol/L NaCl, and 0.1% OGP). For Western blot analysis, the crude supernatant as well as unbound and eluted fractions were subjected to SDS-PAGE. FITC labeling of recombinant cav-1 proteins was prepared with the EZ-label FITC

Requests for reprints: Timothy C. Thompson, The University of Texas M. D. Anderson Cancer Center, Department of Genitourinary Medical Oncology, Unit 1374, 1515 Holcombe Boulevard, Houston, TX 77030. Phone: 713-792-9955; Fax: 713-792-9956; E-mail: timthomp@mdanderson.org.

doi:10.1158/0008-5472.CAN-07-2668

protein labeling kit (Pierce Biotechnology, Inc.) according to the manufacturer's instructions.

Tubule formation assay. The *in vitro* tubule formation assay was used as described previously (12). Briefly, endothelial cells were incubated in growth factor–reduced Matrigel-coated 24-well plates in 0.5 mL of endothelial basement medium (EBM; Cambrex) in the presence or absence of rcav-1 or Δrcav-1. Images of tubule structures that formed after 18 to 24 h were captured by phase contrast microscopy, and the length of the endothelial network was quantified by image analysis of five low-power fields using free object quantification software (NucleoTech Corp.).

Wound-healing migration assay. Endothelial cells were cultured in 24-well plates to 70% to 80% confluency in EGM, and a straight longitudinal incision was made on the monolayer. After a wash with EBM and incubation with rcav-1 or Δrcav-1 in EBM containing 0.1% bovine serum albumin (BSA) for 4 h followed by an additional 48 h of incubation in EBM containing 2% of fetal bovine serum (FBS), the cells were stained with the Protocol HEMA3 stain set (Biochemical Sciences, Inc.), and the number of cells migrating into the cleared area were counted with a microscope, using advanced colony counting software (NucleoTech Corp.).

Cell proliferation and [^{3}H]-thymidine incorporation. Endothelial cells were seeded into 12-well plates (5×10^4 cells per well) and incubated overnight. After the medium was removed, the cells were treated with rcav-1 in EBM for 4 h and incubated for an additional 48 h in EBM containing 2% FBS, after which they were trypsinized and counted with a coulter counter. For [^{3}H]-thymidine uptake, the endothelial cells were seeded into 96-well plates (2.5×10^3 cells per well) in EGM then treated with rcav-1 and incubated for 48 h in EGM. [^{3}H]-thymidine (5 μCi/mL) was then added, the cells were incubated for 24 h, and the cell lysate-associated radioactivity was counted.

Nitric oxide determination. The basal and rcav-1 stimulated NO derived from endothelial cells that had accumulated in EBM over a 24-h period was measured with the Nitric Oxide Colorimetric Assay (Roche Diagnostics).

PP1 and PP2A activities. Endothelial cells were treated with rcav-1 and incubated in EBM containing 0.1% BSA for 24 h at 37°C and 5.5% CO_2. The cells were lysed with ice-cold phosphatase lysis buffer, and PP1 and PP2A activities were measured after immunoprecipitation as described previously (13).

Animal models. Orthotopic RM-9 tumors were generated by injecting 5×10^3 cells directly into the dorsolateral prostates of *cav-1*$^{+/+}$ or *cav-1*$^{-/-}$ male mice. The resultant tumors were removed at necroscopy on day 21 postinjection, and their wet weight were determined; all tumors were processed for specific immunostaining protocols (see below).

To generate the LNCaP cav-1 tet-on system, we transfected *cav-1*$^{-/-}$ low passage (LP)-LNCaP cells with pTetOn vector (Clontech), isolated stable G418-resistant clones, and screened them in a transient trasfection reporter assay with pTRE2Luc vector according to the manufacturer's protocol with or without 1 μg/mL doxycycline. Clone LNT36, which had the highest induction level, was chosen for the second cotransfection, in which a pTRECav-1 vector containing full-length human *cav-1* cDNA and the pBabeHygro plasmid were used. Double stable G418- and hygromycin-resistant clones were isolated and tested for cav-1 induction in response to the doxycycline (1.0 μg/mL). Clone LNTB25cav, which showed strong induction of cav-1 after addition of doxycycline to the medium and the lowest endogenous expression in the absence of the drug *in vitro*, was used for further *in vivo* studies.

To establish xenografts, we inoculated male nude mice with LNTB25cav cells that were suspended in Matrigel matrix and injected s.c. Tumors were present 21 days after inoculation, and tumor-bearing mice were divided into two groups that were normalized for tumor size. One group was treated with drinking water containing doxycycline (2 mg/mL) and 5% sucrose, whereas the other (control group) was treated with drinking water containing only 5% sucrose. After 21 days, the animals were sacrificed, and the tumor tissues were harvested and either snap frozen in liquid nitrogen or fixed in 10% neutral formalin.

For the *in vivo* metastasis assay, 1×10^6 LNTB25cav cells were injected into the tail veins of male nude mice to establish experimental metastases. Two months after the initial injection, the mice were divided into two groups: one was treated with drinking water containing doxycycline (2 mg/mL) and 5% sucrose and the other (control group) with drinking water containing only 5% sucrose. After a 42-day treatment, the animals were sacrificed and lung tissue was collected, fixed, and analyzed for tumor foci.

Immunohistochemistry and deconvolution microscopy. Depending on the fluorescent protein treatment, LNCaP, PC-3, and TSU-Pr1 tumor cells or endothelial cells were placed on glass coverslips in 24-well plates and incubated overnight in RPMI 1640 or EGM, respectively. After removal of the medium, the cells were washed twice with PBS buffer, then FITC-rcav-1, FITC-Δrcav-1, Alexa fluor 594–labeled cholera toxin B, and transferrin (Invitrogen) were added to medium that contained 0.1% BSA. The cells were incubated for 5 h, rinsed twice with PBS buffer, and fixed in 4% formaldehyde for 5 min at room temperature.

For immunostaining, fixed cells were permeabilized for 5 min with 0.1% Triton X-100 in PBS buffer and blocked with 3% normal horse or goat serum. They were then incubated with primary antibody followed by biotinylated anti-rabbit IgG (Vector Labs) and rhodamine-conjugated streptavidin or FITC-streptavidin (Jackson Immuno Research). Reactions were evaluated with the Delta Vision Deconvolution Microscopy System (Applied Precision, Inc.), in which a Z-series of optical sections (0.15-μm steps) were digitally imaged and deconvolved with the Delta Vision–constrained iterative algorithm to generate high-resolution images.

Mouse model–derived tumor specimens were stained for CD31 (BD Biosciences) using the avidin-biotin-peroxidase complex technique (ABC kit; Vector Lab) as previously described (14). Quantitative analysis of microvessel density was performed on the stained sections. The vascular "hot region" was first identified by low-power screening (magnification, ×40). Vascular counting was then performed on at least five 200× measuring fields (each with a real area of 0.198 mm^2). For each sample, the highest count per field was used.

Dual-immunofluorescence staining was also performed on these tissues. Briefly, after tissue sections were deparaffinized and rehydrated through graded alcohol, they were heated in 0.01 mol/L citrate buffer at pH 6.0 by microwave for 10 min to enhance antigen retrieval. After a 20-min blocking step with 1.5% normal goat serum, the sections were sequentially incubated with polyclonal cav-1 antibody diluted 1:200 for 90 min, followed by biotinylated anti-rabbit IgG and streptavidin-FITC for 30 min each. The sections were rinsed and reblocked in 1.5% normal horse serum for 20 min and incubated in CD31 rat monoclonal antibody followed by Cy-3–conjugated anti-rat IgG for 30 min. The specificity of immunoreactions was verified by replacing the primary antibodies with PBS or with corresponding normal serum. The labeled specimens were evaluated using a Zeiss fluorescence microscope equipped with a video camera (Hamamatsu). Each section was analyzed systematically, field-by-field (300×400 μm^2), over the area of cancer cells. The percentages of cav-1–positive CD31 microvessels were determined for each field for each fluorophore and on superimposed images of both fluorophores with the aid of OPTIMAS (6.0) software.

Statistical analysis. The Mann-Whitney rank test was used to analyze differences in microvessel density within mouse prostate cancer tissues; comparisons of *in vitro* tubule formation, cell migration, phosphatase activity assay, NO release assay, and RM-9 tumor wet weights relied on the unpaired two-sided *t* test. Fisher's exact test was used for the comparison of the metastasis frequency in LNTB25cav-injected mice. All statistical analyses were performed with Statview software (Version 5.0; SAS Institute).

Results

Cav-1 uptake by prostate cancer cells and endothelial cells. We have shown that prostate cancer cells secrete cav-1 possessing antiapoptotic activity that can be suppressed by cav-1–specific antiserum *in vitro* (7). Such antiserum also suppressed metastasis *in vivo*, raising the possibility that secreted cav-1 is taken up by tumor cells or tumor-associated endothelial cells or both. Thus, we treated cav-1–negative LP-LNCaP tumor cells or primary

endothelial cells, isolated from *cav-1*$^{-/-}$ mouse aorta, with conditioned medium collected from cav-1–transfected LP-LNCaP cells or with rcav-1 alone. Western blot analysis showed that cav-1 contained in conditioned medium was taken up by LP-LNCaP cells in a dose- and time-dependent manner, as indicated by the appearance of cav-1 in cell lysates within 1 h and the achievement of maximal intracellular levels 3 h posttreatment (Fig. 1*A*). Rcav-1 protein was also taken up by the LP-LNCaP cells and *cav-1*$^{-/-}$ endothelial cells in a dose-dependent fashion over a 24-h incubation period (Fig. 1*B* and *C*). Rcav-1 uptake by tumor cells (LP-LNCaP, TSU-Pr1, and PC-3) and endothelial cells [human umbilical vascular endothelial cell (HUVEC), and mouse *cav-1*$^{-/-}$ and *cav-1*$^{+/+}$] was further shown by fluorescence and deconvolution microscopy. FITC-rcav-1 uptake by these cells was temperature dependent, with 5 h of incubation at 0°C, abolishing uptake altogether (data not shown). Internalized FITC-rcav-1 was distributed throughout the cytoplasm (Fig. 1*D*).

Lipid raft/caveolae-dependent and clathrin-dependent endocytic pathways are involved in rcav-1 internalization in endothelial cells. To determine the endocytic pathways responsible for rcav-1 internalization, we pretreated HUVEC and *cav-1*$^{+/+}$ or *cav-1*$^{-/-}$ mouse endothelial cells with methyl-β-cyclodextrin (MCD) or chlorpromazine to disrupt the formation of cholesterol-rich raft microdomains or clathrin-coated pits, respectively. Fluorescence microscopy revealed that MCD effectively inhibited FITC-rcav-1 uptake in both types of endothelial cells, whereas chlorpromazine inhibited FITC-rcav-1 uptake effectively in mouse endothelial cells but only marginally in HUVEC (Fig. 2*A*). Under the same conditions, MCD effectively reduced the uptake of cholera toxin B, whereas chlorpromazine reduced the uptake of transferrin substances known to penetrate cells through cholesterol-rich lipid raft and clathrin endocytic pathways, respectively (Fig. 2*B*). These results indicate that internalization of exogenous rcav-1 proceeds through lipid raft/caveolae and clathrin pathways in both HUVEC and mouse endothelial cells, with the former pathway dominant in HUVEC (Fig. 2*A, left*). To directly show that rcav-1 associates with internalized lipid rafts/caveolae to enter endothelial cells, we incubated HUVEC for 5 h with a mixture of FITC-rcav-1 and cholera toxin B and tested for their cellular colocalization. We found that a majority (76%) of the FITC-rcav-1–positive endosomes also contained cholera toxin B (Fig. 2*C*), indicative of a requirement for caveolae and ganglioside G_{M1} lipid rafts in cav-1 penetration of human endothelial cells.

Internalization of rcav-1 is mediated by cav-1 scaffolding domain. Mutagenesis experiments have identified cav-1 scaffolding domain (CSD) residues 82 to 101 as the region responsible for mediating interactions with a number of signaling proteins including the endothelial form of nitric oxide synthase (eNOS), platelet-activating factor receptors, epidermal growth factor, the kinases Src and Fyn, heterotrimeric G protein,

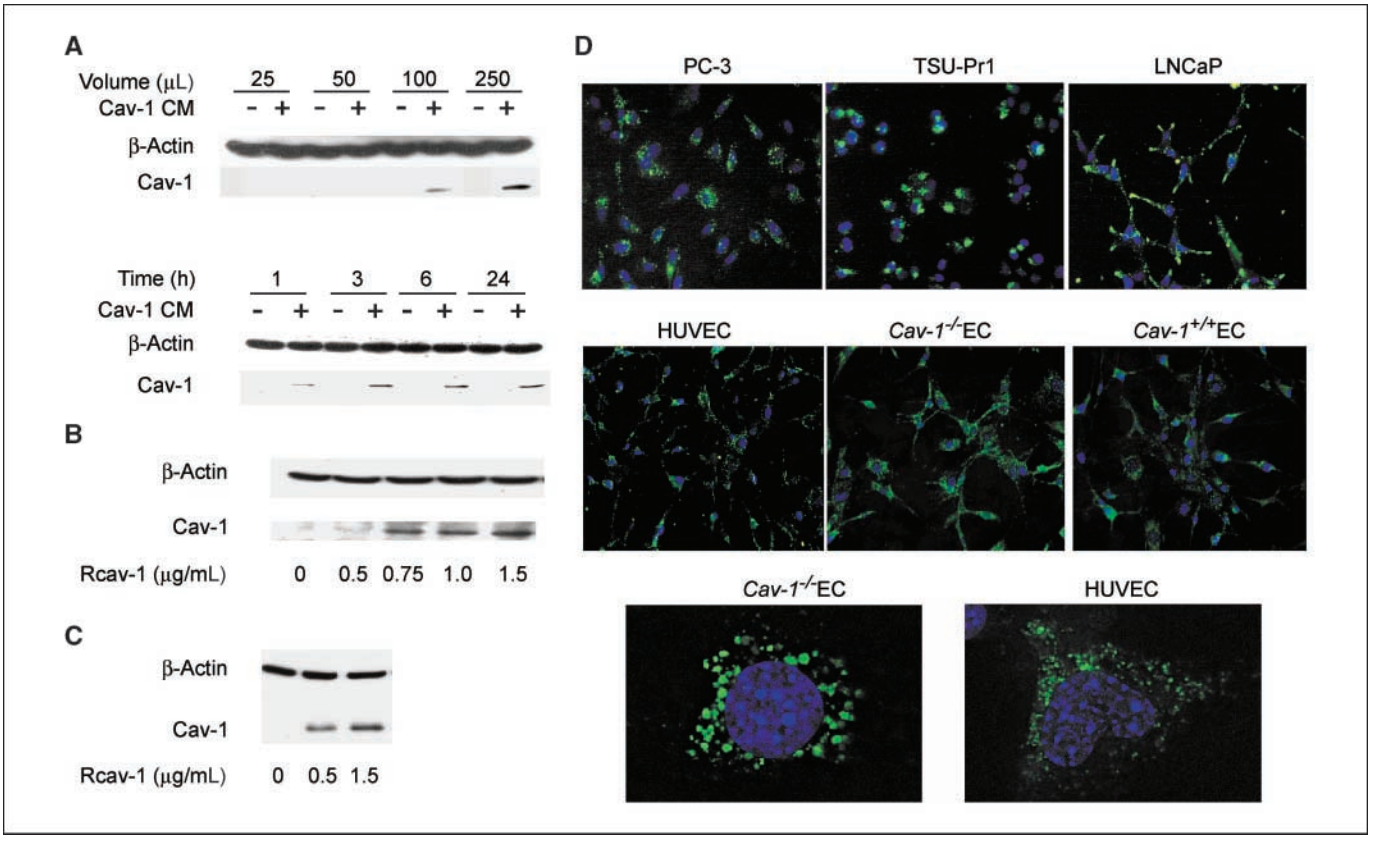

Figure 1. Cav-1 uptake by prostate cancer and bladder cancer cells and endothelial cells. *A,* dose- and time-dependent uptake of cav-1 from *cav-1*–transfected (+) or control-transfected (−) conditioned medium (*CM*) by LP-LNCaP cells. *Top,* detection of cav-1 after a 24-h treatment with conditioned medium over a range of volumes; *bottom,* detection after 1 to 24 h of treatment with 250 μL conditioned medium. *B* and *C,* dose-dependent rcav-1 uptake by LP-LNCaP tumor cells (*B*) and *cav-1*$^{-/-}$ endothelial cells (*EC*; *C*) treated for 24 h. *D,* internalization of FITC-rcav-1 by cancer cells (*top*) and endothelial cells (*middle*) treated with 3.0 μg/mL of FITC-rcav-1 for 5 h. Uptake by endothelial cells (*cav-1*$^{-/-}$ endothelial cells and HUVEC) were imaged by deconvolution microscopy after treatment with FITC-rcav-1 (*bottom*); nuclei were visualized by Hoechst 33342 staining.

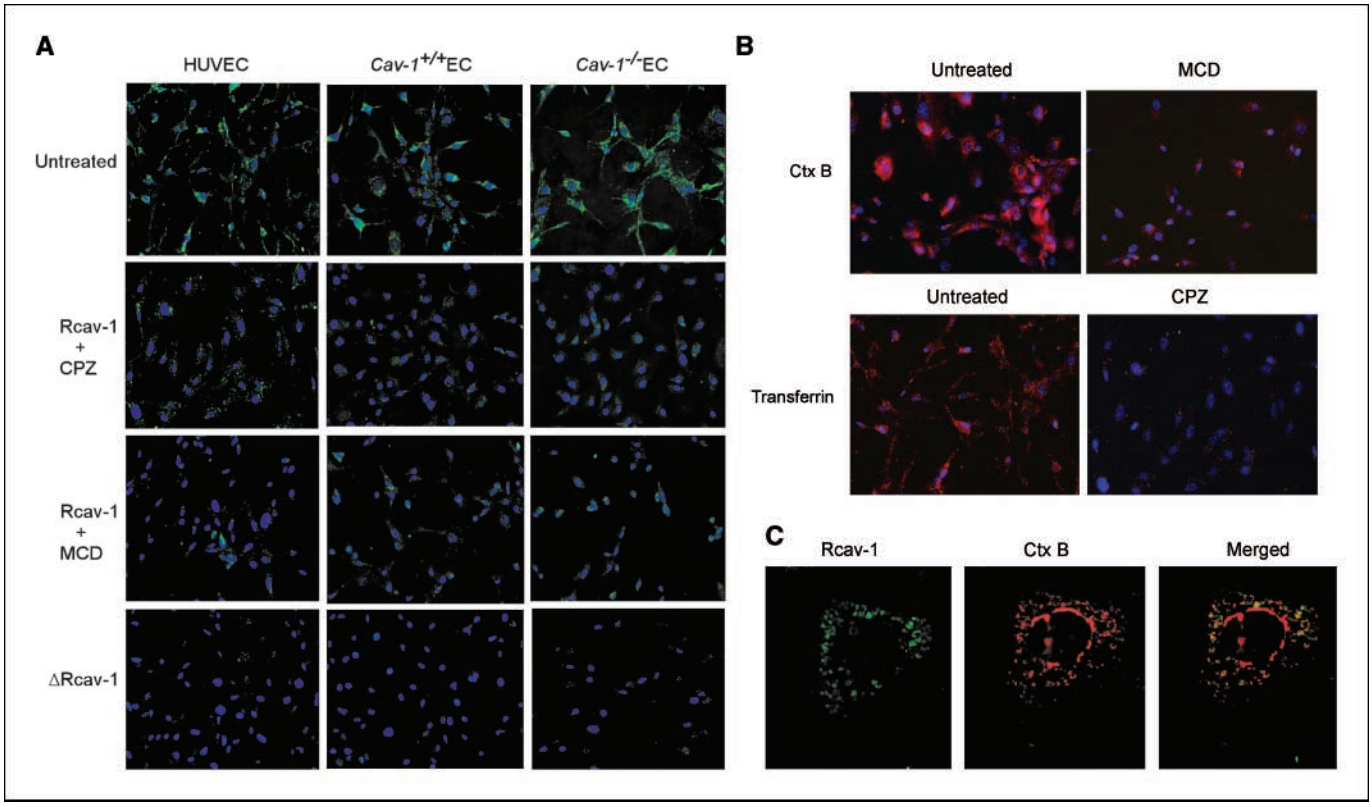

Figure 2. Internalization of rcav-1 by lipid raft/caveolae-dependent and clathrin-dependent endocytic pathways. *A,* cells were incubated with FITC-rcav-1 (3.0 μg/mL) in the presence or absence of 7.5 μg/mL of chlorpromazine (*CPZ*) or 7 mmol/L MCD for 5 h and analyzed by fluorescence microscopy. *B,* cholera toxin B (*Ctx B*) and transferrin internalization are blocked by MCD and chlorpromazine, respectively. HUVEC cells were incubated with Alexa fluor 594–labeled cholera toxin B and transferrin containing the same MCD and chlorpromazine concentrations as in *A* for 5 h and analyzed by fluorescence microscopy. Cholera toxin B internalization was impaired by cholesterol depletion (MCD treatment), whereas transferrin uptake was blocked by disruption of clathrin-coated pits (chlorpromazine treatment). *C,* colocalization of internalized FITC-rcav-1 with cholera toxin B, a ganglioside G_{M1} lipid raft/caveolae marker, as detected by deconvolution microscopy of HUVEC cells after the incubation for 5 h with FITC-rcav-1 and Alexa fluor 594–labeled cholera toxin B; nuclei were visualized by Hoechst 33342 staining.

and cholesterol-binding protein (15). This domain also targets the full-length endogenous cav-1 to lipid rafts/caveolae and cell membranes (16). To determine the role of the CSD in exogenous rcav-1 membrane attachment and cellular uptake, we generated and purified the CSD-deleted rcav-1 protein (Δrcav-1), treated endothelial cells and prostate cancer cells with different concentrations of FITC-Δrcav-1 over 1 to 6 h, and examined the cells for Δrcav-1 uptake using fluorescence microscopy. We did not detect internalized FITC-Δrcav-1 in cells incubated for as long as 6 h at concentrations of the mutant protein ranging to 5.0 μg/mL (Fig. 2*A*). In separate coincubation experiments, we showed uptake of cholera toxin B or transferrin under the same conditions (data not shown). These observations suggest that endocytosis of exogenous rcav-1 protein and its subsequent stimulation of angiogenic activities is mediated, in part, by CSD, which seems critical for cellular internalization of the protein.

Rcav-1 stimulates differentiation and migration of *cav-1*$^{-/-}$ endothelial cells. We initially analyzed the formation of tubules by endothelial cells, isolated from *cav-1*$^{+/+}$ or *cav-1*$^{-/-}$ aorta, on growth factor–reduced Matrigel. Compared with *cav-1*$^{+/+}$ endothelial cells, cells lacking this gene showed significantly reduced tubule formation in the absence of rcav-1 stimulation (Fig. 3*A*; micrographs). However, treatment with rcav-1 stimulated tubule formation in *cav-1*$^{-/-}$ endothelial cells in a dose-dependent manner with a >2-fold increase in tubule length observed with use of 1.5 μg/mL rcav-1 compared with untreated controls (P = 0.021). Importantly, Δrcav-1 at this concentration failed to stimulate tubule formation (Fig. 3*A*). To determine the effects of rcav-1 on *cav-1*$^{-/-}$ endothelial cell migration, we used the *in vitro* wound-healing assay. Rcav-1 treatment stimulated *cav-1*$^{-/-}$ endothelial cell migration in a dose-dependent fashion with a 2-fold increase in the number of migratory cells at a rcav-1 concentration of 1.5 μg/mL (P = 0.019), whereas Δrcav-1 at this concentration failed to increase migration/motility of the endothelial cells (Fig. 3*B*). This enhancement of tubule formation and the number of migratory/motile cells by rcav-1 treatment did not result from increased cell proliferation, as the numbers of cells or levels of thymidine uptake posttreatment were similar to the results for untreated controls (data not shown).

Rcav-1 stimulates the angiogenic activities in *cav-1*$^{-/-}$ endothelial cells through the activation of eNOS. Caveolae and cav-1 play critical roles in ensuring the coupling between vascular endothelial growth factor (VEGF) receptors and downstream mediators of angiogenesis, such as VEGF, which activates Erk and eNOS via the phosphatidylinositol-3-kinase (PI3-K)-Akt signaling pathway (17–19). Thus, to assess the contribution of this signaling module to the angiogenic activities of rcav-1, we tested the effects of inhibitors of PI3 kinase (LY294002), eNOS (L-NAME), and Erk (PD98059) in *cav-1*$^{-/-}$ endothelial cells. Figure 3*C* and *D* shows that both LY294002 and L-NAME, but not PD98059, significantly suppressed rcav-1–stimulated angiogenesis, implicating PI3-K-Akt-eNOS signaling in the pathologic angiogenic effects

of cav-1 in prostate cancer cells. To investigate this possibility further, we measured the levels of accumulated NO (NO_2^- + NO_3^-) at 24 h after rcav-1 treatment of *cav-1*$^{-/-}$ endothelial cells. NO release by these cells was significantly increased by rcav-1 in a dose-dependent manner (P = 0.029 versus untreated control; Fig. 4*A, left*). Analysis of the effects of rcav-1 on the phosphorylation status of Akt and its downstream target protein eNOS in *cav-1*$^{-/-}$ endothelial cells showed a dose-dependent increase in Akt phosphorylation on S473 and T308 with no change in total Akt. Rcav-1 treatment also led to increased eNOS phosphorylation on S1177 but not T495 (Fig. 4*A, right*). The CSD-deleted rcav-1 failed to stimulate eNOS S1177 phosphorylation, as expected (Fig. 4*B, top*). We also tested the effect of LY294002 on the rcav-1–induced phosphorylation of Akt (T308) and eNOS (S1177) in *cav-1*$^{-/-}$ endothelial cells. As expected, LY294002 treatment of the cells diminished the observed Akt phosphorylation induction by rcav-1. Interestingly, the phosphorylation of eNOS (S1177) induced by rcav-1 was reduced but not completely diminished as a result of LY294002 treatment (Fig. 4*B, bottom*).

To further investigate the mechanism(s) that underlies rcav-1–stimulated eNOS activation, we tested the effect of rcav-1 on the activities of serine/threonine protein phosphatases PP1 and PP2A in *cav-1*$^{-/-}$ endothelial cells. These two phosphatases are known to regulate the phosphorylation of multiple protein targets including Akt and eNOS (20, 21) and are inhibited by cav-1 overexpression in prostate cancer cells (13). The activation of eNOS by a number of stimuli including VEGF involves a transient increase in the phosphorylation of S1177 with a decrease in T495 phosphorylation, alternatively, protein kinase C signaling inhibits eNOS activity by phosphorylating T495 and dephosphorylating S1177. Both PP1 and PP2A are associated with eNOS phosphorylation. PP1 is specific for dephosphorylation of T495, whereas PP2A is specific for S1177

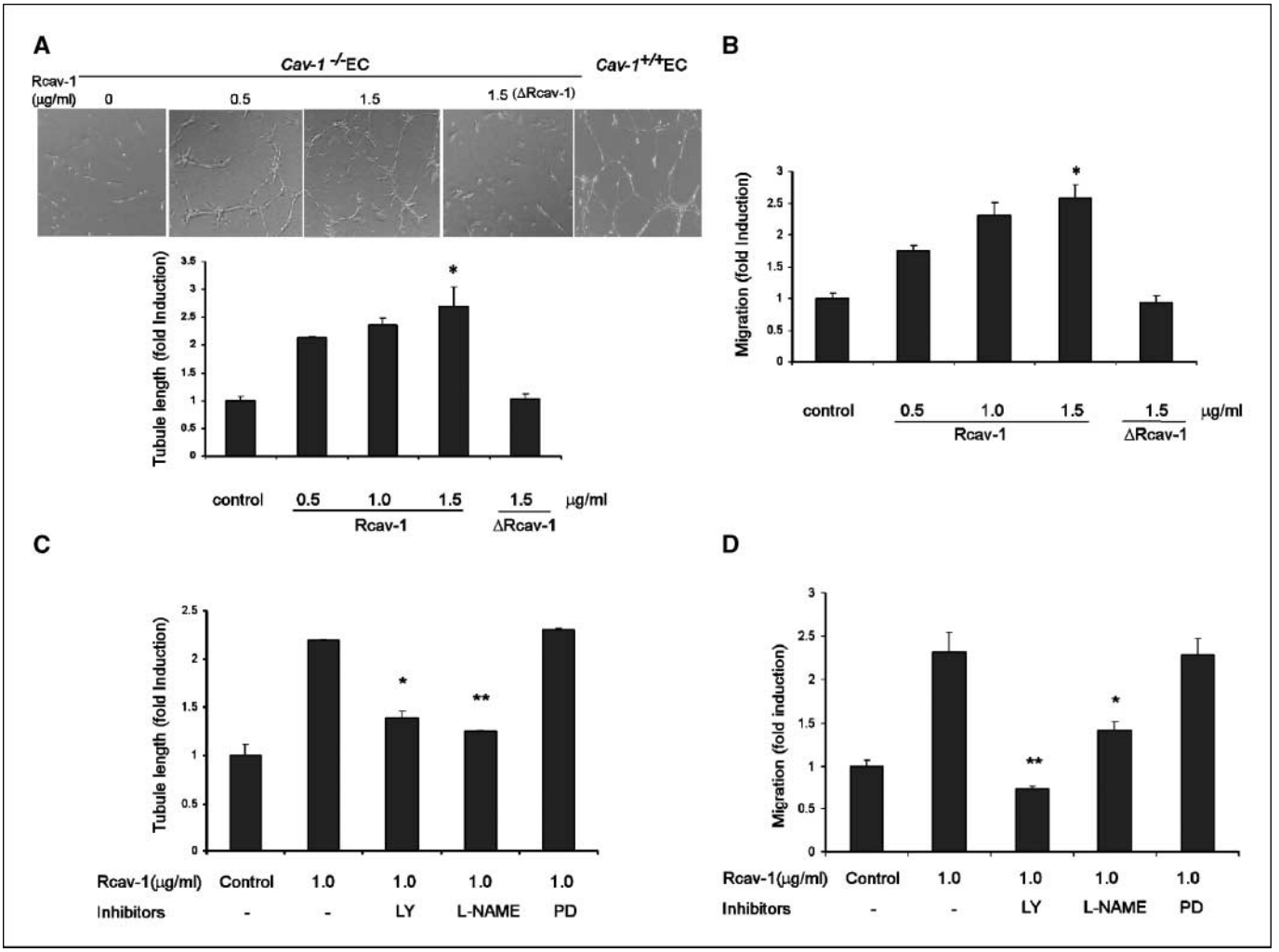

Figure 3. Rcav-1 stimulates tubule formation and cell migration in *cav-1*$^{-/-}$ endothelial cells. *A,* representative micrographs showing newly formed tubules of *cav-1*$^{+/+}$ and *cav-1*$^{-/-}$ endothelial cells cultured on growth factor–reduced Matrigel under basal conditions or after treatment with 0.5 to 1.5 μg/mL of rcav-1 and 1.5 μg/mL Δrcav-1 for 18 h. Bar graph depicts dose-dependent rcav-1 or Δrcav-1 stimulation of tubule formation in *cav-1*$^{-/-}$ endothelial cells. The values are folds of induction relative to untreated control ± SD of three independent experiments. *, P = 0.02 versus untreated control by two-sided t test. *B,* dose-dependent rcav-1 or Δrcav-1 stimulation of *cav-1*$^{-/-}$ endothelial cell migration in a wound-healing assay. The values are folds of induction relative to untreated control ± SD of three independent experiments. *, P = 0.0193 versus untreated control by two-sided t test. *C,* inhibition of rcav-1–stimulated tubule formation by LY294002 (*LY*; 3.0 μmol/L) or L-NAME (1.0 mmol/L) but not by PD98059 (*PD*; 50 μmol/L) in *cav-1*$^{-/-}$ endothelial cells. *, P = 0.008; **, P = 0.003 versus rcav-1 treated only. *D,* inhibition of rcav-1–stimulated wound-healing assay cell migration by LY294002 (3.0 μmol/L) or L-NAME (1.0 mmol/L), but not by PD98059 (50 μmol/L) in *cav-1*$^{-/-}$ endothelial cells. *, P = 0.011; **, P = 0.005 versus rcav-1 treated only, by-two sided t test. Bar graphs in *C* and *D* represent tubule length relative to untreated controls and the number of migratory cells relative to untreated controls, respectively. *Columns,* mean; *bars,* SD.

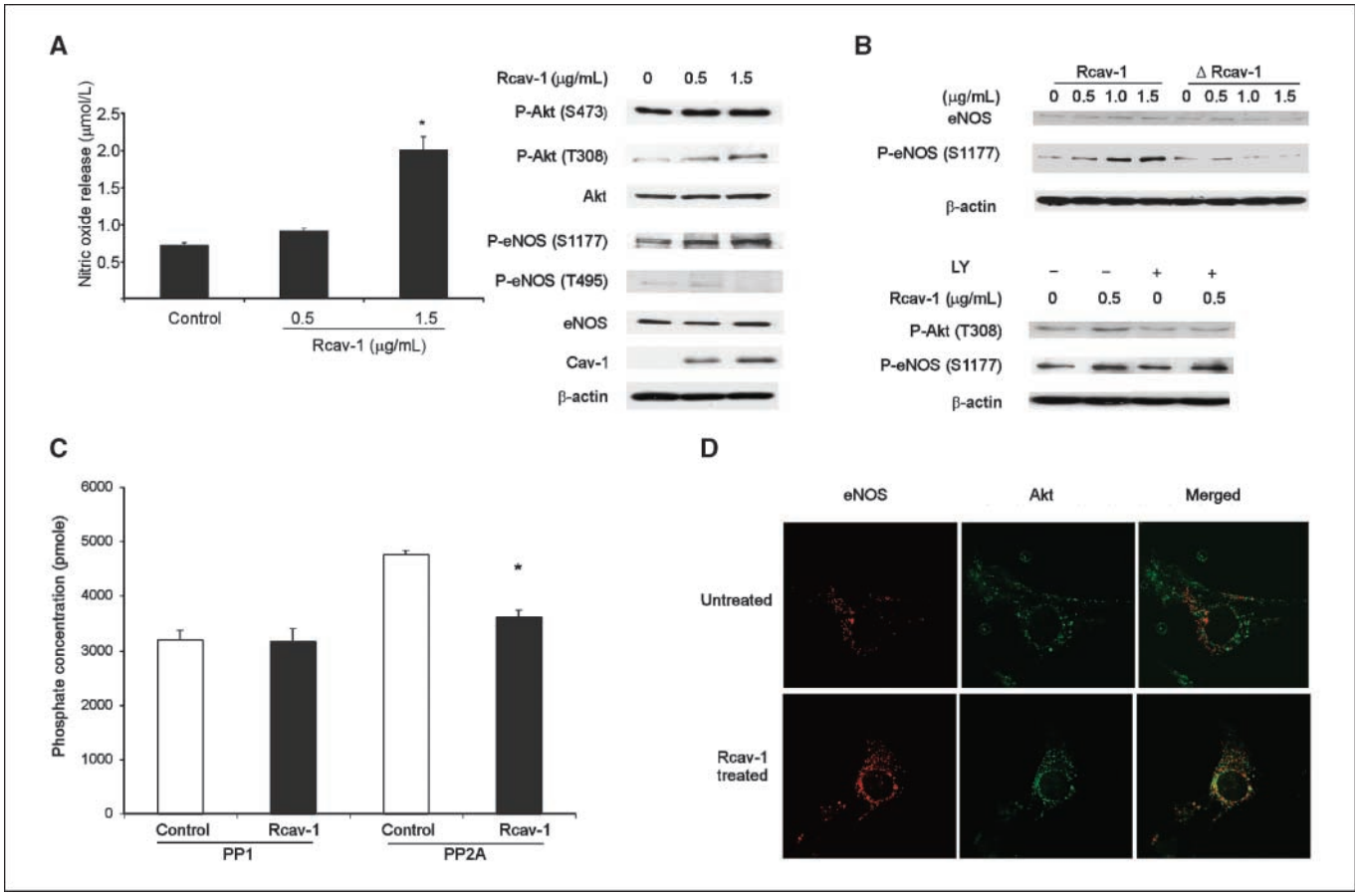

Figure 4. Rcav-1 is involved in PI3-K-Akt-eNOS–mediated stimulation of angiogenic activities in *cav-1*$^{-/-}$ endothelial cells. *A,* dose-dependent NO release by *cav-1*$^{-/-}$ endothelial cells after rcav-1 treatment. *Columns,* mean; *bars,* SD. *, $P = 0.029$ versus untreated control, by two-sided *t* test (*left*). Increased phosphorylation of Akt on S473 and T308, and of eNOS on S1177 by Western blot analysis of *cav-1*$^{-/-}$ endothelial cells lysates treated for 24 h with different concentrations of rcav-1 (*right*). *B,* Δrcav-1 treatment of *cav-1*$^{-/-}$ endothelial cells for 24 h does not affect the phosphorylation status of eNOS on S1177, but rcav-1 increases eNOS phosphorylation on S1177 in a dose-dependent fashion (*top*). Treatment of *cav-1*$^{-/-}$ endothelial cells with LY29400 abolishes the rcav-1–induced Akt phosphorylation on T308 and reduces, but does not completely eliminate, the eNOS phosphorylation on S1177 induced by rcav-1 (*bottom*). *C,* rcav-1 inhibits the activity of PP2A but not PP1 in *cav-1*$^{-/-}$ endothelial cells. PP1-C or PP2A-C immunprecipitation complexes from rcav-1–treated *cav-1*$^{-/-}$ endothelial cells or untreated controls were used to determine phosphatase activities with the serine/threonine protein phosphatase assay. *Columns,* mean; *bars,* SD. *, $P = 0.0002$ by two-sided *t* test. *D*, induction of eNOS/Akt association by rcav-1. *Cav-1*$^{-/-}$ endothelial cells were cultured for 6 h in the presence or absence of rcav-1. After fixation, the cells were double-labeled with anti-eNOS and anti-Akt immunofluorecence. In untreated cells, eNOS (*red*) and Akt (*green*) were localized to separate compartments (*top*), whereas rcav-1 protein treatment of the cells for 6 h induced eNOS (*red*) and Akt (*green*) colocalization in cytoplasmic vesicles (*bottom*), as visualized by deconvolution microscopy.

dephosphorylation (21). The results showed that rcav-1 treatment significantly inhibited the activity of PP2A but had no effect on PP1 activity ($P = 0.0002$ versus control; Fig. 4*C*). These data provide evidence that rcav-1 induces eNOS phosphorylation through Akt activation, and independently of Akt, through inhibition of PP2A, which specifically dephosphorylates eNOS (S1177).

A number of studies have shown that both eNOS and PI3 kinase are colocalized within the caveolar region of the plasma membrane (22, 23); therefore, we investigated the role played by cav-1 in compartmentalization of the PI3-K-Akt-eNOS signaling pathway molecules in *cav-1*$^{-/-}$ endothelial cells. We incubated the cells with or without rcav-1 for 5 h and visualized the cells by deconvolution microscopy for colocalization of Akt with eNOS. We found that Akt was not colocalized with eNOS in untreated cells, whereas significant colocalization of the two molecules was observed in the cells treated with rcav-1 (Fig. 4*D*).

Rcav-1 uptake in tumor-associated endothelial cells and proangiogenic activities in prostate cancer animal models. To investigate the effects of endothelial cells–localized cav-1 on microvessel density and tumor growth *in vivo*, we used an orthotopic RM-9 mouse prostate cancer model (24), in which cav-1 expressing and secreting RM-9 prostate cancer cells are injected directly into the dorsolateral prostate of male *cav-1*$^{+/+}$ or *cav-1*$^{-/-}$ mice. In this model, the mean (1.85 ± 0.167) tumor wet weight was significantly higher in *cav-1*$^{+/+}$ versus *cav-1*$^{-/-}$ mice ($P = 0.045$; Fig. 5*A*). Moreover, immunohistochemical analysis of tumor sections collected from sacrificed mice showed that RM-9 tumors had significantly higher microvessel densities in *cav-1*$^{+/+}$ compared with *cav-1*$^{-/-}$ hosts [median, 21.5 (range, 15.6–36.1) versus 13.3 (range, 8.2–22.8; $P = 0.0078$); Fig. 5*B* and *C*]. Interestingly, >70% of the CD31^{+} microvessels in the *cav-1*$^{-/-}$ mouse tumor sections were positive for cav-1 staining, indicating uptake of RM-9 cell–derived cav-1 by tumor-associated endothelial cells (Fig. 5*D, arrows*).

We examined the association between cav-1 expression and prostate tumor–associated angiogenesis more closely by generating an LNCaP tet-on cav-1 stable cell line (LNTB25cav) in which the expression of cav-1 can be regulated by manipulating doxycycline. In the absence of doxycycline, the level of cav-1 protein in lysate is low, whereas the addition of doxycycline to the culture medium

leads to a rapid induction of cav-1 protein *in vitro* (Fig. 6*A*). LNTB25cav tumors were established as s.c. growing xenografts in adult male nude mice; tumor-bearing mice were then treated with either doxycycline or control sucrose solution added to the drinking water. Tumor volumes in the doxycycline-treated group were significantly greater than those in the control group on days 12, 15, and 18 after treatment ($P = 0.0195$, $P = 0.035$, $P = 0.019$, respectively; Fig. 6*A*). Further immunohistochemical analysis showed increased cav-1 levels in the cytoplasm of tumor cells in doxycycline-treated compared with control mice (Fig. 6*B, top*). Microvessel densities determined by CD31 labeling were greater in cav-1–induced tumors compared with controls ($P = 0.039$; Fig. 6*B, bottom*; Fig. 6*C*). In separate experiments, we injected 1×10^6 LNTB25cav cells into the tail veins of nude mice to establish experimental lung metastases. After 42 days of continuous treatment, the number and frequency of lung metastases in doxycycline-treated animals significantly exceeded results in the control group ($P = 0.008$ and 0.04, respectively; Fig. 6*D*) and their average size was clearly larger in doxycycline-treated mice (data not shown).

Discussion

The establishment of prostate cancer metastases involves the successful negotiation of multiple endogenous physiologic barriers, survival during transit through the blood or lymphatic stream, and colonization at distant sites. The growth and metastasis of prostate cancer and other tumors is dependent on the induction of new blood vessels from preexisting ones through angiogenesis (25, 26). Cav-1 has been implicated in the regulation of endothelial cells proliferation, differentiation, and stabilization (6, 17, 27, 28). In a study using Lewis lung carcinoma cells animal cancer model, cav-1 was found to be antiangiogenic factor (29). In contrast, the results of a number of studies including this report have shown a proangiogenic function for cav-1. In an experimental melanoma model, impairment of pathologic angiogenesis was reported in *cav-1*$^{-/-}$ compared with *cav-1*$^{+/+}$ (30). Increased expression of cav-1 and microvessel density was found to be associated with metastasis and a worse prognosis in human clear cell renal cell carcinoma, suggesting a proangiogenic role for cav-1 (31). We also presented correlative evidence for a proangiogenic role of cav-1 in human prostate cancer (4). Endogenous levels of cav-1 expression in endothelial cells may provide an explanation for this controversy. C*av-1*$^{-/-}$ endothelial cells showed abrogated tubule formation and reduced NO production with or without VEGF treatment. Enforced expression of relatively low levels of cav-1 in cav-1$^{-/-}$ endothelial cells produced increased eNOS phosphorylation (S1177) and NO production in response to VEGF treatment, yet expression of higher levels of cav-1 blocked this process (17).

Apparently, without cav-1, endothelial cells do not undergo proper maturation and maintain a hyperproliferative state. This

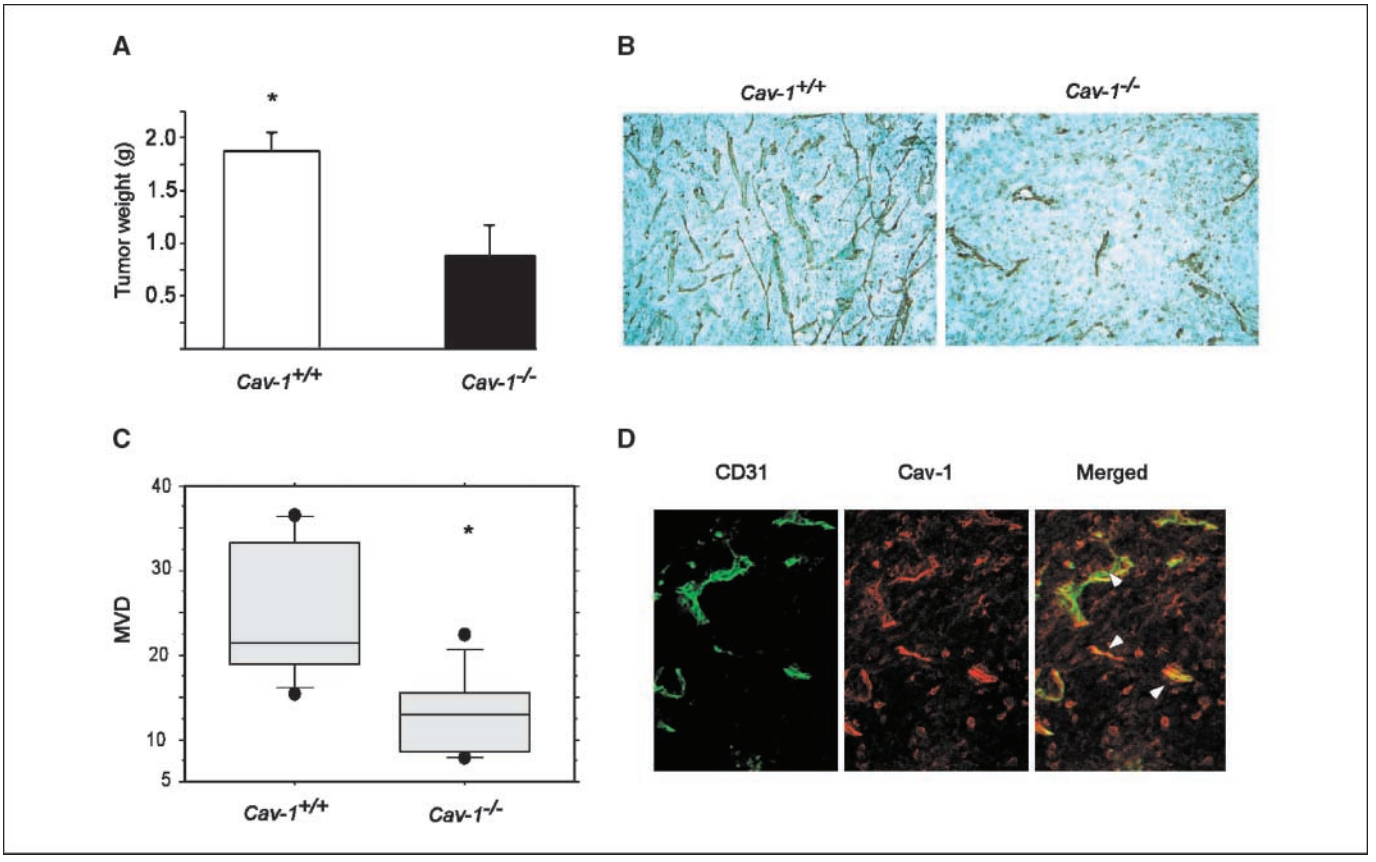

Figure 5. Secreted cav-1 promotes growth and angiogenesis in orthotopic RM-9 mouse prostate cancer model. *A,* increased RM-9 tumor wet weight in *cav-1*$^{+/+}$ hosts ($n = 7$) compared with *cav-1*$^{-/-}$ hosts ($n = 7$). *Columns,* mean; *bars,* SE. *, $P = 0.045$ by two-sided *t* test. *B,* immunohistochemical staining for CD31 in RM-9 tumors shows increased microvessel density in *cav-1*$^{+/+}$ hosts compared with *cav-1*$^{-/-}$ hosts. *C,* quantitative box plot analysis of the microvessel density (*MVD*) in RM-9 tumors from *cav-1*$^{+/+}$ versus *cav-1*$^{-/-}$ hosts. *Top lines,* 10th percentile; *bottom lines,* 90th percentile; *middle lines,* median value. *, $P = 0.0078$ by Mann-Whitney rank test. *D,* images of double immunostaining for CD31 (*green*) and cav-1 (*red*) in a tissue section of an RM-9 tumor from a *cav-1*$^{-/-}$ host. Arrows in the merged image (*yellow*) indicate the uptake by microvessels of cav-1 secreted by RM-9 tumors.

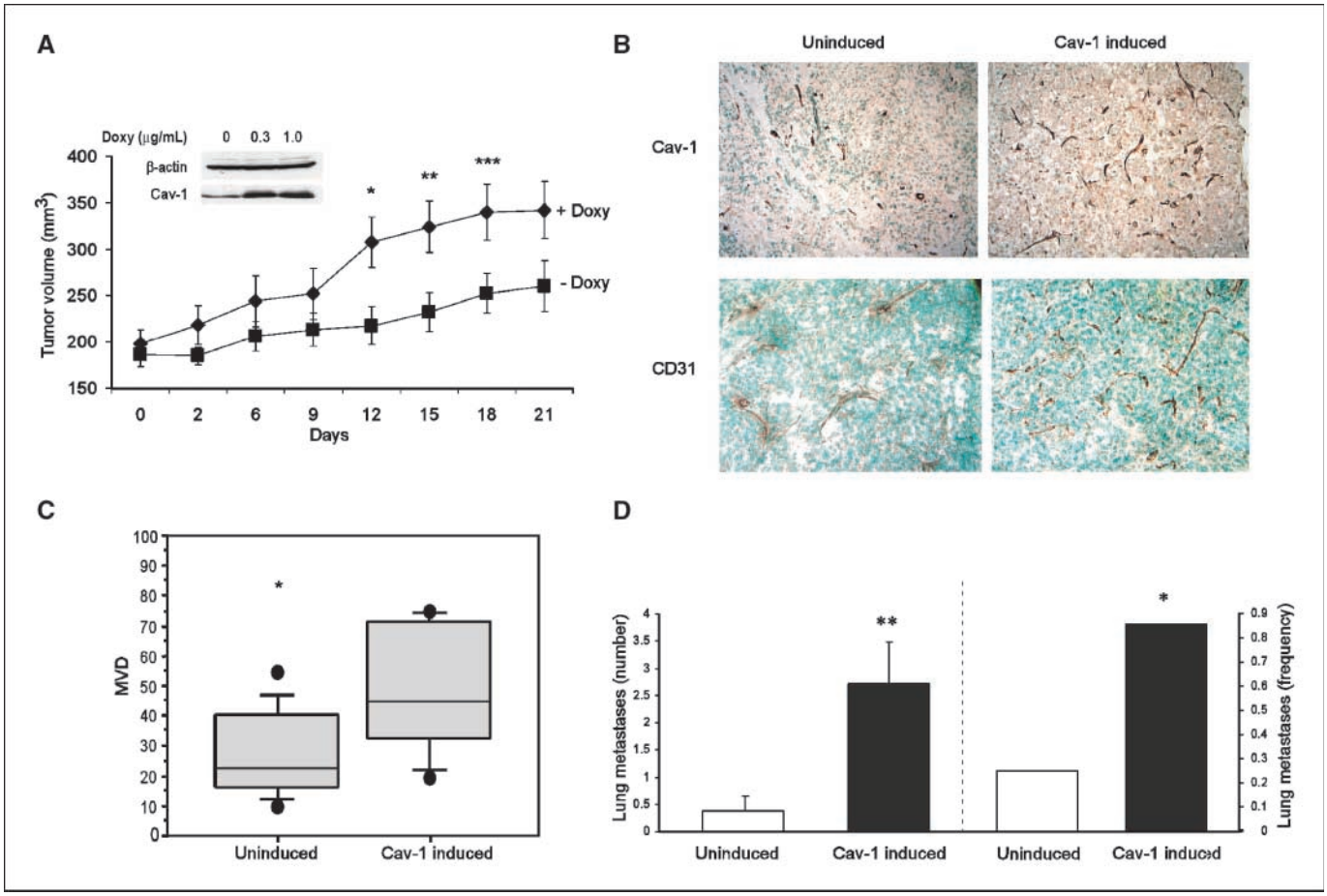

Figure 6. Secreted cav-1 promotes growth and angiogenesis in LNTB25cav tumors. *A,* Cav-1 induction by doxycycline (*Doxy*) leads to increased tumor volume in LNTB25cav s.c xenograft tumors growing s.c. Two groups of mice (n = 8 each) normalized for tumor volume were treated with either doxycycline (2 mg/mL) or control sucrose in drinking water for 21 d. *Points,* mean; *bars,* SE. *, P = 0.0195; **, P = 0.035; ***, P = 0.019 by two-sided t test. *B,* representative immunohistochemical staining for cav-1 and CD31 shows increased cytoplasmic cav-1 in cancer cells (*top*), and increased numbers of microvessels (*bottom*) in cav-1–induced LNTB25cav tumors compared with uninduced LNTB25cav tumors. *C,* quantitative box plot analysis of microvessel density in cav-1–induced (n = 8) and uninduced (n = 11) tumors. *Top lines,* 10th percentile; *bottom lines,* 90th percentiles; *middle lines,* median value. *, P = 0.039 by Mann-Whitney rank test. *D,* increased number and frequency of lung metastases in cav-1–induced compared with uninduced tumors. Lung metastases were established by injecting LNTB25cav cells into the tail veins of nude mice that were subsequently treated with doxycycline (n = 7) or sucrose (n = 8) in drinking water for 42 d. *Columns,* mean; *bars,* SE. *, P = 0.040 by Fisher's exact test; **, P = 0.008 by two-sided t test.

leads to a lack of polarization and a failure to form intercellular junctions (32), which may compromise selective transport mechanisms for specific macromolecules. Similarly, in tumor-associated endothelial cells a certain basal level of cav-1 may be required for minimal functional capacity. We have recently shown that cav-1 low/negative endothelial cells are relevant to prostate cancer. We reported significant reduction in the density of cav-1 positive microvessels in cav-1–negative human prostate cancer tissue compared with benign prostate tissues, clarifying the existence and possible significance of cav-1–negative microvessels in these malignancies (4).

We show that endocytosis of extracellular rcav-1 occurs in cancer cells (TSU-Pr1, DU145, and PC-3) and endothelial cells (HUVEC, *cav-1*$^{-/-}$ endothelial cells, and *cav-1*$^{+/+}$ endothelial cells), and that endothelial cells take up rcav-1 through lipid rafts/caveolae and clathrin-dependent pathways. Our results also show that rcav-1 uptake does not have an absolute cellular requirement for caveolae. The involvement of multiple endocytic pathways is not unique to cav-1 internalization, as these mechanisms have been described for the internalization of a number of proteins such as protein-specific membrane antigen (33), insulin growth factor binding protein-3 (34), transforming growth factor β receptor (35), and decorin (36). A possible explanation for the internalization of cav-1 through multiple pathways is its ability to interact with and bind to a large number of signaling proteins including multiple membrane receptors (15), which places it in proximity to endosome-forming activities of various pathways.

We show that CSD is necessary but may not be sufficient for cav-1 uptake, which leads to tubule formation, cell migration, and NO production in *cav-1*$^{-/-}$ endothelial cells. These data are supported by the results of a study that identified a highly conserved region of the engrailed homeoproteins that bears a high degree of homology with the CSD and are responsible for oligopeptide or oligonucleotide transmembrane, and cellular transport (37). The CSD was also found to have the ability to direct endogeneous cav-1 to cell membranes (16).

We show that cav-1 angiogenic activities involve the PI3-K-Akt-eNOS pathway but not Erk1/2. Indeed, rcav-1 treatment increases phosphorylation of Akt (S473 and T308) and, hence, eNOS phosphorylation (S1177 but not T495), leading to NO production.

Because previous studies show that Akt phosphorylates eNOS on the S1177 site, leading to eNOS activation, our results are consistent with a straight forward molecular pathway through which cav-1 uptake activates Akt, which in turn activates eNOS. However, Akt inhibitor studies indicated that Akt signaling is not the only pathway culminating in eNOS phosphorylation on S1177. That is, rcav-1–stimulated Akt activation was accompanied by inhibition of PP2A, a specific serine/threonine kinase that dephosphorylates S473 and T308 on Akt, and S1177 and T495 on eNOS (13, 21, 38). It is of interest that rcav-1 did not inhibit PP1, a serine/threonine kinase whose substrate specificity is similar to that of PP2A. Because PP1 may have selective activity for the T495 site on eNOS, which unlike the S1177 site leads to inhibition of eNOS activity, the absence of cav-1–mediated inhibition of PP1 could further contribute to eNOS activation (21). This notion is supported by the absence of increased phosphorylation of T495 on eNOS in response to rcav-1 (Fig. 4*A, right*). Because we previously showed that cav-1–stimulated PP1, and PP2A inhibition is mediated through direct interaction between the cav-1 CSD and PP1/PP2A binding sites in prostate cancer cells, (13) it seems reasonable to suggest that this specific interaction also applies to rcav-1–mediated inhibition of PP2A in *cav-1*$^{-/-}$ endothelial cells.

Studies with two complementary animal model systems (i.e., the RM-9-*cav-1*$^{-/-}$ host orthotopic model and the LNTB25cav xenograft model) substantiate our *in vitro* findings that tumor-associated endothelial cells internalize tumor-secreted cav-1, which is associated with tumor growth, and that overexpression of cav-1 in prostate cancer cells promotes angiogenesis and tumor growth.

Overall, our data show that prostate cancer cell–derived and prostate cancer cell–secreted cav-1 has autocrine (tumor cell uptake) and paracrine (tumor-associated endothelial cells uptake) activities that can contribute to angiogenesis, tumor progression, and metastasis. We propose that prostate cancer and potentially other malignancies that overexpress and secrete cav-1, may benefit from anti–cav-1 therapy that could involve cav-1 antibodies or peptide inhibitors of CSD.

Acknowledgments

Received 7/13/2007; revised 9/27/2007; accepted 11/12/2007.

Grant support: NIH grants RO1 CA68814 and Specialized Programs of Research Excellence P50 58204 and DAMD PC051247 from the Department of Defense.

The costs of publication of this article were defrayed in part by the payment of page charges. This article must therefore be hereby marked *advertisement* in accordance with 18 U.S.C. Section 1734 solely to indicate this fact.

References

1. Shaul PW, Anderson RG. Role of plasmalemmal caveolae in signal transduction. Am J Physiol 1998;275: L843–51.

2. Nasu Y, Timme TL, Yang G, et al. Suppression of caveolin expression induces androgen sensitivity in metastatic androgen-insensitive mouse prostate cancer cells. Nat Med 1998;4:1062–4.

3. Yang G, Truong LD, Timme TL, et al. Elevated expression of caveolin is associated with prostate and breast cancer. Clin Cancer Res 1998;4:1873–80.

4. Yang G, Addai J, Ayala G, et al. Correlative evidence that prostate cancer cell-derived caveolin-1 mediated angiogenesis. Hum Pathol 2007;38:1688–95.

5. Williams TM, Lisanti MP. The Caveolin genes: from cell biology to medicine. Ann Med 2004;36:584–95.

6. Carver LA, Schnitzer JE. Caveolae: mining little caves for new cancer targets. Nat Rev Cancer 2003;3: 571–81.

7. Tahir SA, Yang G, Ebara S, et al. Secreted caveolin-1 stimulates cell survival/clonal growth and contributes to metastasis in androgen-insensitive prostate cancer. Cancer Res 2001;61:3882–5.

8. Tahir SA, Ren C, Timme TL, et al. Development of an immunoassay for serum caveolin-1: a novel biomarker for prostate cancer. Clin Cancer Res 2003;9:3653–9.

9. Tahir SA, Frolov A, Hayes TG, et al. Preoperative serum caveolin-1 as a prognostic marker for recurrence in a radical prostatectomy cohort. Clin Cancer Res 2006;12: 4872–5.

10. Williams TM, Hassan GS, Li J, et al. Caveolin-1 promotes tumor progression in an autochthonous mouse model of prostate cancer: genetic ablation of Cav-1 delays advanced prostate tumor development in TRAMP mice. J Biol Chem 2005;10:1074.

11. Cao G, Yang G, Timme TL, et al. Disruption of the caveolin-1 gene impairs renal calcium reabsorption and leads to hypercalciuria and urolithiasis. Am J Pathol 2003;162:1241–8.

12. Brouet A, Sonveaux P, Dessy C, et al. Hsp90 and caveolin are key targets for the proangiogenic nitric oxide-mediated effects of statins. Circ Res 2001;89: 866–73.

13. Li L, Ren CH, Tahir SA, Thompson TC. Caveolin-1 maintains activated Akt in prostate cancer cells through scaffolding domain binding site interactions with and inhibition of serine/threonine protein phosphatases PP1 and PP2A. Mol Cell Biol 2003;23:9389–404.

14. Vermeulen PB, Gasparini G, Fox SB, et al. Second international consensus on the methodology and criteria of evaluation of angiogenesis quantification in solid human tumours. Eur J Cancer 2002;38:1564–79.

15. Smart EJ, Graf GA, McNiven MA, et al. Caveolins, liquid-ordered domains, and signal transduction. Mol Cell Biol 1999;19:7289–304.

16. Schlegel A, Lisanti MP. A molecular dissection of caveolin-1 membrane attachment and oligomerization. Two separate regions of the caveolin-1 C-terminal domain mediate membrane binding and oligomer/oligomer interactions *in vivo*. J Biol Chem 2000;275: 21605–17.

17. Sonveaux P, Martinive P, DeWever J, et al. Caveolin-1 expression is critical for vascular endothelial growth factor-induced ischemic hindlimb collateralization and nitric oxide-mediated angiogenesis. Circ Res 2004;95: 154–61.

18. Labrecque L, Royal I, Surprenant DS, et al. Regulation of vascular endothelial growth factor receptor-2 activity by caveolin-1 and plasma membrane cholesterol. Mol Biol Cell 2003;14:334–47.

19. Liu J, Wang XB, Park DS, Lisanti MP. Caveolin-1 expression enhances endothelial capillary tubule formation. J Biol Chem 2002;277:10661–8.

20. Cohen PT. Protein phosphatase 1-targeted in many directions. J Cell Sci 2002;115:241–56.

21. Michell BJ, Chen Z, Tiganis T, et al. Coordinated control of endothelial nitric-oxide synthase phosphorylation by protein kinase C and the cAMP-dependent protein kinase. J Biol Chem 2001;276:17625–8.

22. Chambliss KL, Shaul PW. Rapid activation of endothelial NO synthase by estrogen: evidence for a steroid receptor fast-action complex (SRFC) in caveolae. Steroids 2002;67:413–9.

23. Stirone C, Boroujerdi A, Duckles SP, Krause DN. Estrogen receptor activation of phosphoinositide-3 kinase, akt, and nitric oxide signaling in cerebral blood vessels: rapid and long-term effects. Mol Pharmacol 2005;67:105–13.

24. Nasu Y, Bangma C, Hull G, et al. Combination gene therapy with adenoviral vector-mediated HSV-tk+GCV and IL-12 in an orthotopic mouse model for prostate cancer. Prostate Cancer Prostatic Diseases 2001;4:44–55.

25. Hanahan D, Folkman J. Patterns and emerging mechanisms of the angiogenic switch during tumorigenesis. Cell 1996;86:353–64.

26. Carmeliet P, Jain RK. Angiogenesis in cancer and other diseases. Nature 2000;407:249–57.

27. Frank PG, Woodman SE, Park DS, Lisanti MP. Caveolin, caveolae, and endothelial cell function. Arterioscler Thromb Vasc Biol 2003;23:1161–8.

28. Massimino ML, Griffoni C, Spisni E, Toni M, Tomasi V. Involvement of caveolae and caveolae-like domains in signalling, cell survival and angiogenesis. Cell Signal 2002;14:93–8.

29. Lin MI, Yu J, Murata T, Sessa WC. Caveolin-1-deficient mice have increased tumor microvascular permeability, angiogenesis, and growth. Cancer Res 2007;67:2849–56.

30. Woodman SE, Ashton AW, Schubert W, et al. Caveolin-1 knockout mice show an impaired angiogenic response to exogenous stimuli. Am J Pathol 2003;162: 2059–68.

31. Joo HJ, Oh DK, Kim YS, Lee KB, Kim SJ. Increased expression of caveolin-1 and microvessel density correlates with metastasis and poor prognosis in clear cell renal cell carcinoma. BJU Int 2004;93:291–6.

32. Razani B, Engelman JA, Wang XB, et al. Caveolin-1 null mice are viable but show evidence of hyperproliferative and vascular abnormalities. J Biol Chem 2001;276:38121–38.

33. Anilkumar G, Barwe SP, Christiansen JJ, et al. Association of prostate-specific membrane antigen with caveolin-1 and its caveolae-dependent internalization in microvascular endothelial cells: implications for targeting to tumor vasculature. Microvasc Res 2006; 72:54–61.

34. Lee KW, Liu B, Ma L, et al. Cellular internalization of insulin-like growth factor binding protein-3: distinct endocytic pathways facilitate re-uptake and nuclear localization. J Biol Chem 2004;279:469–76.

35. Di Guglielmo GM, Le Roy C, Goodfellow AF, Wrana JL. Distinct endocytic pathways regulate TGF-β receptor signalling and turnover. Nat Cell Biol 2003;5:410–21.

36. Feugaing DD, Tammi R, Echtermeyer FG, et al. Endocytosis of the dermatan sulfate proteoglycan decorin utilizes multiple pathways and is modulated by epidermal growth factor receptor signaling. Biochimie 2007;89:637–57.

37. Joliot A, Trembleau A, Raposo G, et al. Association of engrailed homeoproteins with vesicles presenting caveolae-like properties. Development 1997;124: 1865–75.

38. Urbich C, Reissner A, Chavakis E, et al. Dephosphorylation of endothelial nitric oxide synthase contributes to the anti-angiogenic effects of endostatin. FASEB J 2002;16:706–8.